Assessing the quantification of acetylation in konjac glucomannan via ATR-FTIR and solid-state NMR spectroscopy

Kash Bhullar, Michael I.M. Horgan, Ashley Le, David Fania, Richard Wuhrer, Valentina Razmovski-Naumovski, Kelvin Chan, Patrice Castignolles, Marianne Gaborieau

Highlights

- Konjac glucomannan (KGM) is not fully soluble in common aqueous and organic solvents,

- Degree of acetylation, *DA*, was assessed in KGM by solid-state spectroscopy,

- Acetylation was assessed quickly, qualitatively, by FTIR in outer layer of particles,

- The first meaningful quantification of *DA* was achieved in the solid state by ^{13}C NMR,

- *DA* ranged from 4 to 8 % of the hexoses in selected KGM samples.

Graphical abstract

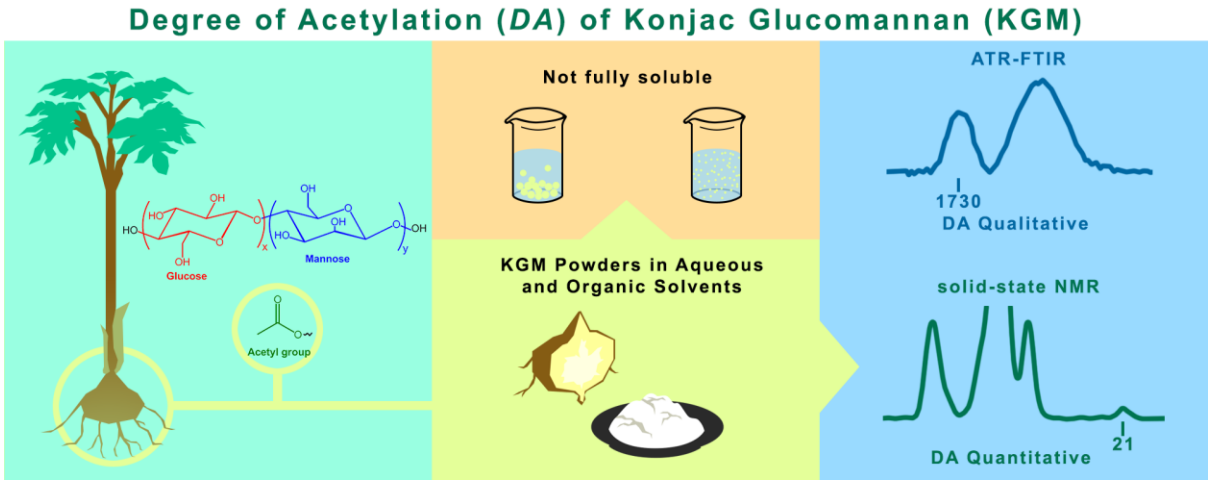

Assessing the Quantification of Acetylation in Konjac Glucomannan via ATR-FTIR and Solid-state NMR Spectroscopy

Kash A. Bhullar [a], *Michael I. M. Horgan* [a], *Ashley Le* [a], *David Fania* [b], *Richard Wuhrer* [b], *Valentina Razmovski-Naumovski* [c,d], *Kelvin Chan* [c,e], *Patrice Castignolles* [a,f,♦,**], *Marianne Gaborieau* [a,♦,1]

[a] Western Sydney University, Australian Centre for Research on Separation Science (ACROSS), School of Science, Parramatta Campus, Locked Bag 1797, Penrith NSW 2751, Australia

[b] Western Sydney University, Advanced Materials Characterisation Facility, Parramatta Campus, Locked Bag 1797, Penrith NSW 2751, Australia

[c] Western Sydney University, NICM Health Research Institute, School of Science, Campbelltown Campus, Locked Bag 1797, Penrith NSW 2751, Australia

[d] South West Sydney Clinical Campuses, Discipline of Medicine, University of New South Wales Sydney, NSW 2170, Australia

[e] Liverpool John Moores University, School of Pharmacy & Biomolecular Sciences, Liverpool L3 3AF, United Kingdom

[f] Sorbonne University, Parisian Institute of Molecular Chemistry, UMR 8232, Polymer Chemistry team, 75252 Paris, France

Abstract

Dietary fiber like konjac glucomannan (KGM) is important in maintaining good human health. There is no established method for quantifying the average degree of acetylation *DA* of this polysaccharide. Polysaccharides are notoriously difficult to dissolve. In this study, KGM could

♦ Members of the European Polysaccharide Network of Excellence (EPNOE)
[1] Corresponding Author.
** Correspondence to: Prof. Patrice Castignolles, Dr Marianne Gaborieau. E-mail addresses: patrice.castignolles@sorbonne-universite.fr, m.gaborieau@westernsydney.edu.au

not be fully dissolved in common solvents and was characterized in the solid state. ATR-FTIR spectroscopy enabled a fast qualitative assessment of acetylation, selective to the outer layer of KGM particles, and identifying excipients like magnesium stearate. Average *DA* was quantified for the first time with solid-state ^{13}C NMR in KGM: semi-quantitative measurements on the same arbitrary scale by cross polarization (1 to 2 days) were calibrated with a few longer single-pulse excitation measurements (approximately 1 week). *DA* values ranged from 4 to 8 % of the hexoses in the backbone, in agreement with previously reported values. This method could be used for quality control and standardization of KGM products.

Keywords

Konjac glucomannan; Degree of acetylation; Quantification; Solubility; Solid-state NMR spectroscopy; ATR-FTIR spectroscopy

[2]

1. Introduction

Glucomannan is a neutral polysaccharide abundant in plant bulbs, tubers or softwoods (Alonso-Sande, Teijeiro-Osorio, Remunan-Lopez & Alonso, 2009; Gidley, McArthur & Underwood, 1991). The most commonly used and studied glucomannan is konjac glucomannan (KGM) (Chua, Baldwin, Hocking & Chan, 2010; Rinaudo, 2006). It is extracted from the root of *Amorphophallus konjac* K. Koch (Araceae), a tuber plant native to Southeast and East Asia (Chua et al., 2010). There, it has been used as a food source and as a traditional medicine (Chua

[2] Abbreviations

ATR-FTIR: attenuation total reflectance Fourier-transform infrared; CP: cross polarization; *DA*: degree of acetylation; DMAc: *N*-*N*-dimethyl acetamide; DMSO: dimethyl sulfoxide; KGM: Konjac glucomannan; MAS; magic-angle spinning; NMR: nuclear magnetic resonance spectroscopy; *RSD*: relative standard deviation; SEC: size-exclusion chromatography; *SNR*: signal-to-noise ratio (of signal A in ^{13}C NMR spectra); SPE: single-pulse excitation.

et al., 2010). KGM is increasingly researched for its desirable properties: it is inexpensive, biodegradable, biocompatible, and able to form films and gels (Gomes Neto et al., 2019; Wu et al., 2012). KGM and its derivatives have many applications in the pharmaceutical industry as an excipient (Alonso-Sande et al., 2009), in the food industry as a texture modifier and thickener (Kok, Abdelhameed, Ang, Morris & Harding, 2009), in water purification (Zhu, 2018), in food packaging and cosmetics (Zhang, Xie & Gan, 2005), and potentially in drug delivery (Alonso-Sande et al., 2009). KGM is a dietary fiber and has no calorific content; it is thus used as a satiety agent and as an ingredient in low-calorie foods (Chua et al., 2010; Singh, Singh & Arya, 2018) and can potentially treat obesity-related disorders (Chua et al., 2010; Keithley & Swanson, 2005). However, its incomplete characterization at the molecular level affects the quality control of the products.

The structure proposed (Figure 1) is a hetero-polysaccharide composed of β(1,4) linked D-glucose and D-mannose, with branching and acetylation (Alonso-Sande et al., 2009; Kato & Matsuda, 1969; Kok et al., 2009). Mannose-to-glucose ratios are reported at about 1.6. Branching with short side chains is reported to occur at the C-3 position of some hexoses or at the C-6 position of some glucose residues. Acetylation is reported to occur at the C-6 position of 5 to 10 % of the hexoses. The weight-average molar mass of KGM reported from size-exclusion chromatography (SEC) coupled to multi-angle light scattering detection is typically 10^4 to 2×10^6 g.mol^{-1} (Alonso-Sande et al., 2009; Kok et al., 2009; Ratcliffe, Williams, Viebke & Meadows, 2005). Branching and the presence of different monomer units (different hexoses) may affect the separation by SEC and thus, the determined molar masses (Gaborieau & Castignolles, 2011).

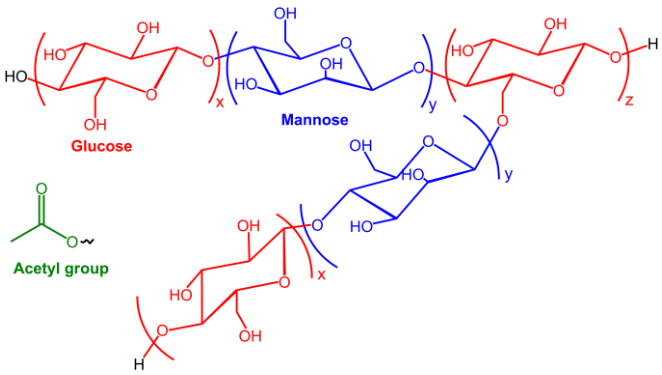

Figure 1: Schematic representation of KGM structure composed of glucose (red) and mannose (blue) units with acetylation and branching. The acetyl group (green) was reported to be at the C-6 position on some of the hexoses (CH_2-O-H becoming CH_2-O-acetyl).

Complete molecular dissolution is required for a successful separation and meaningful characterization of molecules in solution, with techniques like chromatography, SEC or nuclear magnetic resonance spectroscopy (NMR). It is also required for a homogeneous chemical modification. Complete dissolution is usually assumed when a clear, transparent solution is obtained but this is not sufficient to prove complete dissolution as aggregates (i.e., microgels) may be present (Maniego, Sutton, Gaborieau & Castignolles, 2017; Schmitz, Dona, Castignolles, Gilbert & Gaborieau, 2009; Thevarajah, Bulanadi, Wagner, Gaborieau & Castignolles, 2016a). Polysaccharides are notoriously difficult to dissolve (Rebiere et al., 2016; Schmitz et al., 2009; Thevarajah et al., 2016a). KGM's numerous hydrogen bonds make its dissolution difficult in aqueous (Alonso-Sande et al., 2009) and organic solvents (El Seoud, Koschella, Fidale, Dorn & Heinze, 2007; Ratcliffe et al., 2005). Water is a poor solvent for konjac glucomannan (Kruk, Kaczmarczyk, Ptaszek, Goik & Ptaszek, 2017). Homogeneous KGM dispersions have been reported using sonication or microwave irradiation; however, this causes degradation (Ratcliffe et al., 2005). Studies reporting homogeneous dispersions using water, aqueous cadoxen (CdO/ethylenediamine) (Nishinari, 2000) and NaOH/thiourea (Yang, Xiong & Zhang, 2002), have not confirmed KGM's complete dissolution.

Since the 1920s, the complex KGM structure has been investigated using different methods (Katsuraya et al., 2003; Kok et al., 2009; Nishinari, Williams & Phillips, 1992) with the 1980s introducing solution-state NMR (Brigden & Wilkinson, 1985). ^{1}H solution-state NMR measurements showed acetyl groups on mannose and glucose units (Williams et al., 2000). However, it is rarely mentioned whether the NMR spectra presented are quantitative or if the samples were fully soluble. Thus, solid-state methods (e.g., spectroscopy) should be used for a reliable analysis of the whole sample. Solid-state NMR can characterize polymers at the molecular level in terms of average composition, packing and chain dynamics (Spiess, 2017). Chain conformations and impurities (lipids, proteins) in 'dry', hydrated powders and gels of KGM were analyzed by solid-state ^{13}C NMR (Felix da Silva et al., 2020; Gidley et al., 1991). Solid-state ^{13}C NMR of KGM exhibits sufficient resolution for identifying acetylation (Felix da Silva et al., 2020); however, insufficient information was provided to judge whether the spectra were quantitative.

Attenuation total reflectance Fourier transform infrared (ATR-FTIR) spectroscopy is cheaper and faster than solid-state NMR. KGM was qualitatively analyzed by ATR-FTIR spectroscopy, with bands in the 1800-800 cm^{-1} region originating from glucose, mannose units and acetyl

groups (Felix da Silva et al., 2020); however, quantification has been limited, due to signal overlap and difficulty in obtaining quantitative data.

Variability in KGM's composition, structure and size has been reported between studies depending on analytical procedures (Alonso-Sande et al., 2009). Acetylation is a relevant property to measure as it affects KGM's solubility in water, the viscosity of its dispersions, and its gelation behavior (Alonso-Sande et al., 2009; Du, Li, Chen & Li, 2012; Kok et al., 2009; Williams et al., 2000). Therefore, the aim of the study is to quantify the average degree of acetylation *DA* in KGM. The research questions addressed in the present work are: (a) whether konjac glucomannan is soluble in common solvents, and (b) whether ATR-FTIR and solid-state NMR spectroscopy can quantify acetylation in KGM if solubility is incomplete.

2. Material and methods

2.1. Materials

Milli-Q quality water (Millipore, Bedford, MA, USA) was used. Sodium hydroxide pellets (98 %, NaOH), dimethyl sulfoxide (≥99.5 %, DMSO), lithium bromide (99 %, LiBr), sodium chloride (99.5 %, NaCl), *N*,*N*-dimethyl acetamide (≥99.5 %, DMAc), acetic anhydride (99 %), ethanol (99 %), and adamantane (99 %) were from Sigma-Aldrich. Singly ^{13}C-labelled alanines (1-^{13}C, 2-^{13}C, or 3-^{13}C; 99 %) were from Cambridge Isotope laboratories, Inc. Anhydrous DMSO was produced using molecular sieves (208582, 3Å, 8-12 mesh beads from Sigma-Aldrich). Soluble starch powder was from Fisons (Homebush, NSW, Australia). Glucose powder (Dextrose, bacteriological grade) was from Oxid Ltd, London. KGM samples are described in Table 1.

Table 1: KGM samples used in the study.

Sample	Description	Product name, supplier	Batch number	Composition (as listed by supplier)
KGMA	Powder*	Konjac Glucomannan Excel Slim Fiber M&S Colloid Technology Ltd., Hong Kong, China	T-4255	KGM 100 %
KGMB	Powder#	100% Pure Glucomannan Powder, NOW Foods Ltd., Bloomingdale, Illinois, USA	6513 V2	KGM 100 %

KGMC	Powder[#]	Fiber dense Glucomannan, Swanson Health Products, Inc., Fargo, ND, USA	SW1163	KGM, gelatin, rice flour, microcrystalline cellulose, magnesium stearate, silica
KGMD	Powder[#]	Double Strength Glucomannan, Puritan's Pride, INC. Holbrook, NY, USA	B36120 01B	KGM, gelatin, vegetable magnesium stearate
KGME	Powder*	Luralean® Glucomannan Powder (Grade A), AHD International, Atlanta, Georgia, USA	GC1212 31A	KGM 100 %
KGMF	Powder*	Glucomannan Luralean® medium, Nutra Novus, Atlanta, Georgia, USA	121224 RS	KGM 100 %
KGMG	Powder*	Arkocaps Konjac, Arkopharma laboratories pharmaceutiques, Carros, France	CCP148 9A	KGM, hydroxypropyl methylcellulose, magnesium stearate
KGMS ∞	Wet, long, pasta-like*	Slendier Slimpasta Spaghetti, D'Lite FoodPacific Pty Ltd, Mt Waverley, Victoria, Australia	2013	KGM, starch, gelatin

* from corm, [#] from root

∞ not included in acetylation assessment since only available as gel-like pasta (not solid).

2.2. Methods

2.2.1. Dissolution tests

Samples (starch, glucose, KGM except KGMG) were prepared at nominal concentrations of 0.625 $g.L^{-1}$, 0.5 $g.L^{-1}$and/or 0.1 $g.L^{-1}$ in different solvents: aqueous (water, water with 5 % NaCl, with 98 % NaCl, with 0.01 M NaOH or with 0.1 M NaOH) and organic (DMSO, DMSO with 98 % LiBr, anhydrous DMSO, anhydrous DMSO with 5 % LiBr, anhydrous DMSO with 98 % LiBr, DMAc, DMAc with 5 % LiBr), where percentages are weight/weight (w/w). All samples were prepared in 2 mL flat-bottom glass vials, heated at 80 °C for 3 h in a water bath, and briefly taken out for visual observation every hour (more details in supplementary material).

2.2.2. KGM acetylation

KGMB acetylation into KGMB-ac followed a published method (Koroskenyi & McCarthy, 2001). Briefly, KGMB powder (1.0 g), acetic anhydride (10 mL) and sodium hydroxide

aqueous solution (50 % (w/w)) were stirred in a round-bottom flask (50 mL) for 3 h at room temperature under reflux. The sample was vacuum filtered, washed with ethanol and freeze-dried.

2.2.3. FTIR spectroscopy

The FTIR spectra of powder samples were recorded with a 2 cm^{-1} resolution and 64 scans using a Bruker Vertex 70 spectrometer with a diamond ATR window crystal; the data treated and normalized using the Bruker OPUS software suite (unless specified). A background was measured before each measurement. For quantification, 10 replicate ATR-FTIR spectra were collected for each sample; spectra were treated with ATR correction, smoothing over 25 points, and baseline correction with 51 iterations. The precision was assessed through the standard deviation of the 10 *DA* values determined from the replicate spectra for each sample.

2.2.4. Solid-state NMR spectroscopy

Solid-state ^{1}H and ^{13}C NMR spectra were recorded on a Bruker DPX200 spectrometer operating at Larmor frequencies of 200 MHz and 50 MHz for ^{1}H and ^{13}C, respectively. A commercial double-resonance, magic-angle spinning (MAS) probe was used. Samples were spun at the magic angle at 10 kHz (for single pulse excitation, SPE) and 12 kHz (for cross polarization, CP) in rotors with a 4-mm outer and a 3-mm inner diameter. For ^{1}H and ^{13}C SPE-MAS experiments, the 90° pulse was optimized using adamantane; for ^{13}C CP-MAS experiments power levels were optimized using a mixture of three ^{13}C singly labelled alanine. The ^{1}H and ^{13}C chemical shifts scales were externally referenced to the CH resonance of adamantane at 1.64 and 38.48 ppm, respectively (Morcombe & Zilm, 2003).

^{1}H NMR spectra were recorded using a 5 µs 90° pulse length, a 3 s repetition delay and at least 32 scans. ^{13}C CP-MAS NMR spectra of KGMA were recorded with 0.2, 0.5, 1 and 2 ms contact times, with a 5 s repetition delay and 8192 scans, then recorded with 3, 4, 5, 5.5, 6, and 7 ms contact times, with a 5 s repetition delay and 32768 scans. ^{13}C CP-MAS NMR experiments of KGMB, KGMB-ac, KGMC, KGMD, KGME, KGMF and KGMG were recorded with a 5.5 ms contact time, a 5 s relaxation delay and 32769 scans. Quantitative ^{13}C SPE-MAS spectra were recorded for KGMA, KGMB, KGMB-ac and KGME with a 100 s repetition delay (at least five time longer than T_1 for signals A to D), using 90° pulse lengths of 3.75, 4.25, 4.25 and 4.15 µs, respectively, with 4096, 3111, 7534 and 4427 scans, respectively. The signal-to-

noise ratio (*SNR*) was determined with the 'sino cal' function of Bruker Topspin 3.2, with signal in the range of 15-30 ppm, and noise over the range of 200-340 ppm with a 40-ppm range.

3. Results & Discussion

Original data of this study (FTIR and NMR data) are available at Mendeley Data (http://dx.doi.org/10.17632/y26t6t7wvz.2).

3.1. Visual observation of dissolution

To date, no complete molecular dissolution of native KGM has been reported. In this study, visual observation revealed incomplete dissolution of KGM in aqueous media after 3 h at 80 °C while (visually) complete dissolution occurred for glucose and soluble starch in the same conditions (Table S3 in supplementary material). KGM strongly interacts with water through its numerous hydroxy groups. Acetyl groups replace hydroxy groups on KGM, making the polysaccharide more hydrophobic and thus, could be expected to make it less water-soluble. However, acetylation is reported to increase KGM's water-solubility (Alonso-Sande et al., 2009; Stephen & Churms, 2006). In this study, KGM concentration in water was decreased from 0.625 to 0.5 then to 0.1 $g.L^{-1}$ to promote KGM solvation by decreasing the proximity of KGM chains in solution. KGM dispersions in water exhibited aggregates visible as particles at higher concentrations, while smaller aggregates resulted in turbidity of the dispersion at lower concentrations. Salt (NaCl) was added to water to promote the disruption of the hydrogen bonds which are preventing KGM dissolution, following an approach that was successful with starch (Schmitz et al., 2009). NaCl had no visible effect on KGM solubility at lower salt concentration (5 %) and a negative effect at higher salt concentration (98 %) with some samples exhibiting an increase in the size of the particles visible in the dispersion. pH was then increased to promote the disruption of the hydrogen bonds. At higher KGM and lower NaOH concentration (0.01 M), KGM solubility slightly improved, with no changes observed at lower KGM and higher NaOH concentration (0.1 M). NaOH addition has been reported to promote KGM dissolution but also its deacetylation, leading to KGM gelation (Huang, Takahashi, Kobayashi, Kawase & Nishinari, 2002). Aqueous solvents tested in this study were unable to completely dissolve KGM, thus organic solvents commonly used for polysaccharide dissolution were tested.

KGM dissolution was visually incomplete in organic media after 3 h at 80 °C, while dissolution was (visually) complete for glucose and soluble starch in some of these conditions (Table S4). This was unexpected for KGM, as similar complex polysaccharides, like starch, have dissolved in DMSO-based solvents (Schmitz et al., 2009). Adding LiBr as a hydrogen bond disruptor to DMSO did not visually improve KGM dissolution; neither did using DMAc (without or with LiBr), another solvent commonly used for cellulose dissolution (Furuhata, Koganei, Chang, Aoki & Sakamoto, 1992).

Thus, KGM was not fully soluble in the solvents tested (aqueous or organic). At best, very fine dispersions were formed. A meaningful characterization of KGM in solution was therefore not possible. Methods that characterize solid-state samples were thus chosen for assessing acetylation.

3.2. ATR-FTIR spectroscopy

The acetyl group is observed in FTIR spectra of KGM through the characteristic band of its stretching vibration ν(C=O) at 1730 cm^{-1} (Chua et al., 2012) (see Table S5 for complete signal assignment). FTIR data acquisition and treatment were first examined with the intensity and resolution of this band in mind (Figures S2 to S5). Although transmission FTIR overcame the limited penetration depth of the irradiation in the sample (about 2 μm (Sevenou, Hill, Farhat & Mitchell, 2002) in ATR-FTIR), it provided insufficient resolution for the signal at 1730 cm^{-1} (Figure S3 and S4). For quantification, ATR-FTIR data was analyzed with ATR correction, smoothing over 25 points, and baseline correction with 51 iterations (Figure 2).

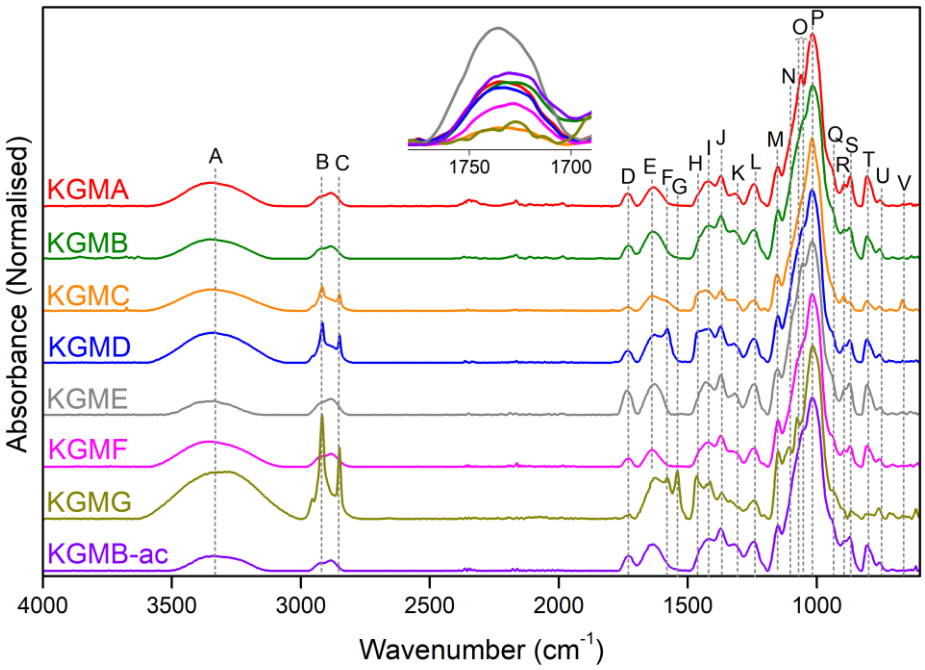

Figure 2: ATR-FTIR spectra of KGM samples (see Table S5 for signal assignment).

The FTIR bands most relevant to KGM's acetylation are from carbonyl stretching at 1730 cm^{-1}, water molecule in-plane deformation at 1655 cm^{-1}, and ether stretching at 1015 cm^{-1} (labeled D, E and P in Figure 2; see Table S5 for complete signal assignment). The FTIR region of 4000 to 1800 cm^{-1} is similar for all KGM samples, except for sharp bands (B and C) at 2850 and 2920 cm^{-1} showing the presence of magnesium stearate excipient in KGMC, KGMD and KGMG (in larger proportion in KGMG than KGMC or KGMD). The other bands of this excipient at ~3300, 1580, 1465 and 750 cm^{-1} (Table S5), are not expected to interfere with FTIR acetylation studies.

Ten replicate ATR-FTIR spectra were recorded from 1800 to 600 cm^{-1} for each KGM sample (Figures S6 to S13) and were highly repeatable. Quantifying *DA* in KGM requires (1) resolving one band belonging to the acetyl group and one belonging to each hexose as a reference, and (2) extracting the relative ratio of the corresponding functional groups in the sample from their relative intensities. The acetyl band at 1730 cm^{-1} was resolved (Figure 2); however, no hexose bands were fully resolved. It was decided to put all ATR-FTIR spectra on the same "hexose scale" by normalizing them to the same intensity (height) of the most intense band (P) of hexose rings at 1015 cm^{-1}. *DA* was then estimated as DA_{IR} (in arbitrary units a.u.) as the area of the acetyl band D on that arbitrary scale. The precision was assessed from the 10 values determined from replicate spectra for each sample.

DA_{IR} values for KGM samples (except KGMB-ac) ranged from 1.7 to 10.7 a.u. (see Table S8 for values). These are not absolute (quantitative) values: firstly, because the acetyl band areas were normalized with a band height, not a band area, for the hexoses, and secondly, band intensities in FTIR spectroscopy are not directly proportional to the concentration of the corresponding functional groups in the sample. These also depend on extinction coefficients, which were not considered here and may not be known. Nevertheless, qualitative comparisons between samples are possible with this measurement. For example, it was estimated that the acetylation reaction carried out on KGMB to yield KGMB-ac significantly increased its *DA* by 50 to 110 %. The limitations of ATR-FTIR spectroscopy to quantify *DA* in KGM are addressed via the use of solid-state NMR, which presents the advantage of measuring the whole sample.

3.3. Solid-state NMR spectroscopy

3.3.1. ^{1}H vs ^{13}C NMR

Although solid-state ^{1}H NMR is faster (typically minutes) than solid-state ^{13}C NMR (typically hours to days), the method usually exhibits a lower resolution. Solid-state ^{1}H NMR spectra of KGM samples exhibited a broad signal around 3 to 5 ppm (Figure 3a). KGME and KGMG exhibited a broader signal than other samples, indicating a lower mobility of the polymer chains. One narrow, low intensity signal (at 1.1 ppm) was observed for KGMG. This may originate in very mobile molecules which could be low amounts of magnesium stearate excipient (methylene moieties of stearate exhibit their most intense ^{1}H NMR signal at a chemical shift of 1.25 ppm according to a simulation with ChemDraw, Cambridgesoft). Solid-state ^{1}H NMR resolution was insufficient to selectively observe acetyl group signals and thus to investigate acetylation in KGM.

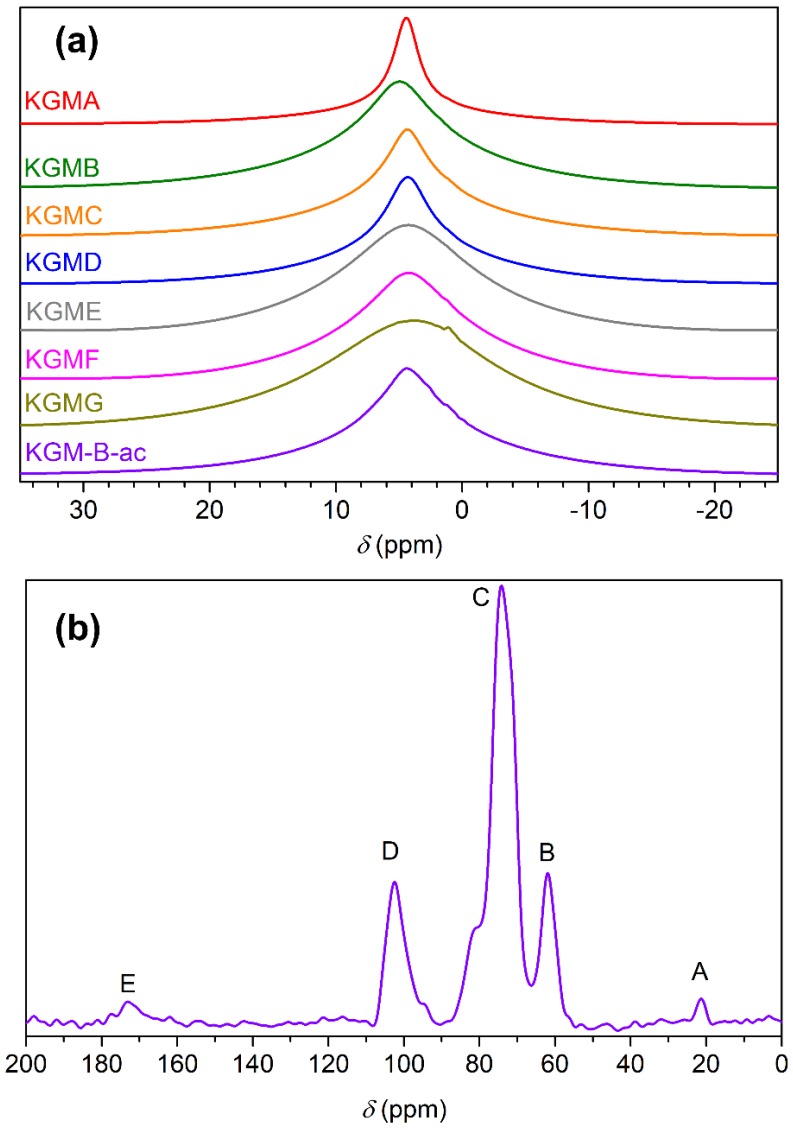

259

260 *Figure 3: (a) Solid-state ^{1}H MAS NMR spectra of all KGM samples and (b) ^{13}C SPE-MAS*
261 *NMR spectrum of KGMB-ac.*

262 Solid-state ^{13}C NMR improved the spectral resolution for KGM (Figure 3b). The ^{13}C SPE-
263 MAS NMR spectrum of KGMB-ac was consistent with published spectra recorded in similar
264 conditions (Gidley et al., 1991; Vieira & Gil, 2005). Signals were resolved for the acetyl group:
265 a methyl signal at 21 ppm and a carbonyl signal at 173 ppm (labeled A and E, respectively, in
266 Figure 3b; see Table S6 for complete signal assignment). The signal at 103 ppm (D in Figure
267 3b) corresponds to one carbon in each of the hexoses. The *DA* can thus, in principle, be
268 quantified in KGM by ^{13}C NMR via integration of signals D and either A or E. However, the
269 limited sensitivity of signals A and E renders quantification difficult as the acquisition of a

quantitative spectrum with good sensitivity would require long measuring times (approximately 1 week for each sample).

3.3.2. Semi-quantitative ^{13}C CP-MAS

^{13}C CP-MAS NMR enabled the measurement of the methyl and carbonyl signals from the acetyl group in a significantly shorter duration (1 to 2 days, Figure 4b) and provided semi-quantitative data (Gaborieau, Nebhani, Graf, Barner & Barner-Kowollik, 2010). Here, semi-quantitative refers to quantifying a ratio of signal intensities with a consistent systematic error so that the ratio is determined on the same arbitrary scale for all samples. This allows comparisons between samples, and the arbitrary scale can also be calibrated. ^{13}C CP-MAS NMR spectra were recorded with different contact times (Figure 4a and Figure S14) to find a range over which the intensity ratio of the signals A and D, or E and D, did not vary significantly (here 5, 5.5 and 6 ms contact times). Therefore, for a semi-quantitative comparison on the same arbitrary scale the ^{13}C CP-MAS spectra were recorded with an intermediate 5.5 ms contact time (Figure 4b).

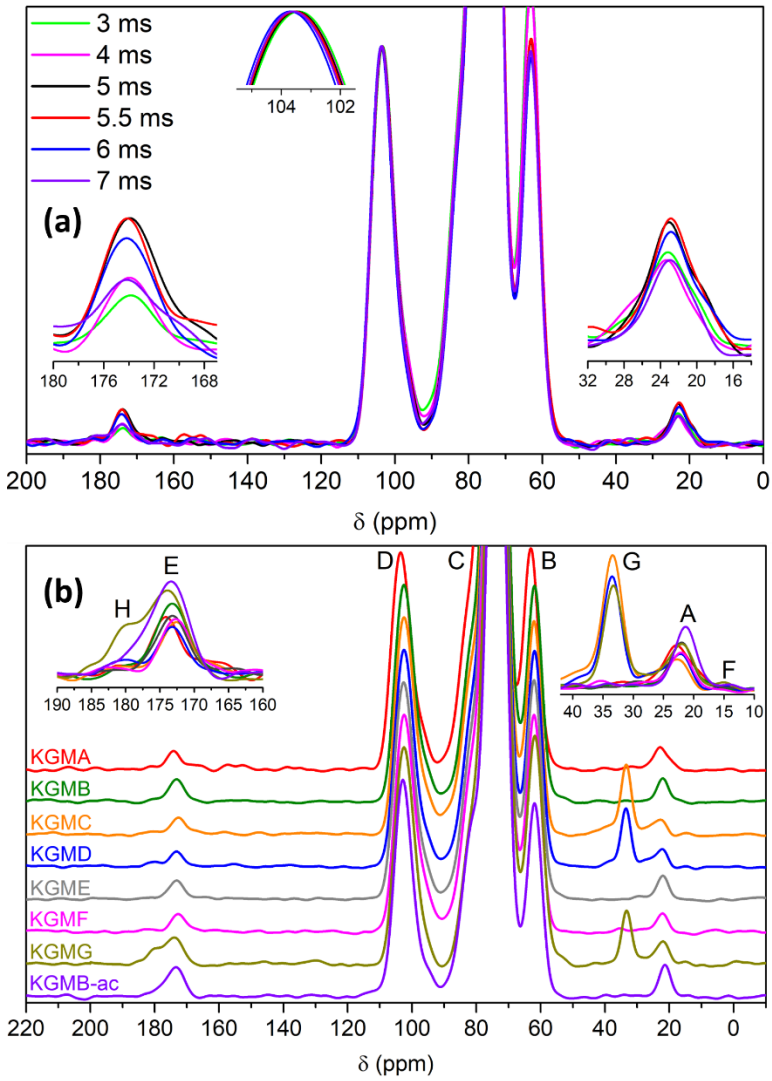

Figure 4: Solid-state ^{13}C CP-MAS NMR spectra (normalized to signal D at 103 ppm) of (a) KGMA with different contact times T_{CP} of 3, 4, 5, 5.5, 6, and 7 ms and (b) all KGM samples with T_{CP} of 5.5 ms.

DA was quantified in all KGM samples from ^{13}C CP-MAS spectra on the same arbitrary scale as the percentage of hexoses bearing an acetyl group using Eq. 1:

$$DA_{CP} = \frac{100 \cdot I_A}{I_D} \quad (1)$$

where I_A is the area of the signal A at 21 ppm from one methyl carbon of each acetyl group, and I_D is the area of the signal D at 103 ppm from one carbon (C-1) of each hexose. It was not practical to do enough replicates of the ^{13}C CP-MAS measurement (each taking approximately a day) to assess the precision of DA_{CP} from them. The precision of the determined DA_{CP} was estimated through an empirical relation (Eq. 2) established for determining degrees of

296 branching in polyacrylates and polyolefins by solid-state ^{13}C NMR (Castignolles, Graf,
297 Parkinson, Wilhelm & Gaborieau, 2009). In determining both *DA* and degree of branching, the
298 ratio of two signal intensities was used, with that of the signal of limited sensitivity on the
299 numerator. This relation is:

300 $$RSD = \frac{238}{SNR^{1.28}} \quad (2)$$

301 where *RSD* is the relative standard deviation of the determined intensity ratio, and *SNR* the
302 signal-to-noise ratio of the signal with limited sensitivity on the numerator (signal A here). The
303 methyl signal A was chosen over the carbonyl signal E since the carbonyl signal H at 182 ppm
304 of the excipient magnesium stearate strongly overlapped with signal E in KGMC, KGMD and
305 KGMG (see Figure 4b for signal labels and Table S6 for signal). In these samples, another
306 magnesium stearate signal (G at 33 ppm) slightly overlapped with signal A. The relative signal
307 intensities confirmed the qualitative purity assessment from FTIR spectroscopy that KGMG
308 contained relatively more magnesium stearate than KGMC or KGME. The signal D at 103 ppm
309 was not fully resolved from the signal C at 76 ppm for all KGM samples (Figure 4b). However,
310 for accurate quantification, full resolution (baseline resolution) of the signals of interest is
311 needed. The resolution R_S of signals A and D, from signals G and C, respectively, was
312 estimated with Eq. 3, typically used in chromatography:

313 $$R_S = \frac{\delta_1 + \delta_2}{\frac{1}{2}(fwhm_1 + fwhm_2)} \quad (3)$$

314 where δ_1 and δ_2 are the chemical shifts of the signals of interest, and $fhwm_1$ and $fwhm_2$ are their
315 full widths at half maximum. For Gaussian lineshapes, full resolution occurs for R_S higher than
316 2. The resolution of signal D (and C) was almost complete, above 3.8 for all KGM samples
317 (Table S7), indicating a very limited impact of the resolution on DA_{CP} determination. The
318 resolution of signal A (and G) was between 2.1 and 2.6 for KGMC, KGMD and KGMG (Table
319 S7), and this may affect DA_{CP} quantification when magnesium stearate is present. The DA_{CP}
320 values of KGM samples (except KGMB-ac) were between 4.4 and 7.9 a.u. (arbitrary units),
321 and the acetylation reaction increased KGMB's *DA* by 25 to 50 % (Table S8).

322 ### *3.3.3. Quantitative ^{13}C SPE-MAS*

323 Following a published approach to calibrate the arbitrary scale (Gaborieau et al., 2010),
324 quantitative ^{13}C SPE-MAS spectra were recorded with sufficiently long delays between scans

to ensure full relaxation. ^{13}C longitudinal relaxation times (T_1) of signals A and D were between 5 and 20 s in KGMB-ac, while the experiment was inconclusive for signal E (Figure S15). Quantitative ^{13}C SPE-MAS spectra of KGMA, KGMB, KGMB-ac and KGME were thus recorded using a relaxation delay of 100 s (Figure 5; these spectra are quantitative for all signals except possibly the carbonyl signal E at 173 ppm). These samples were selected as they do not contain magnesium stearate, which potentially affects *DA* assessment. For good *DA* precision, measuring time was set to ensure a sufficient *SNR* (higher than 4), keeping in mind that *SNR* only increases with the square root of the measuring time. Equations 2 and 3 were used to determine the quantitative DA_{SPE} values for KGMA, KGMB, KGMB-ac and KGME and their *RSD* from the ^{13}C SPE-MAS spectra (Table S8). The quantitative DA_{SPE} values ranged from 4.8 to 7.4 % of the hexoses for the KGM samples (except KGMB-ac), and the acetylation reaction on KGMB increased its quantitative DA_{SPE} value by 33 to 115 %.

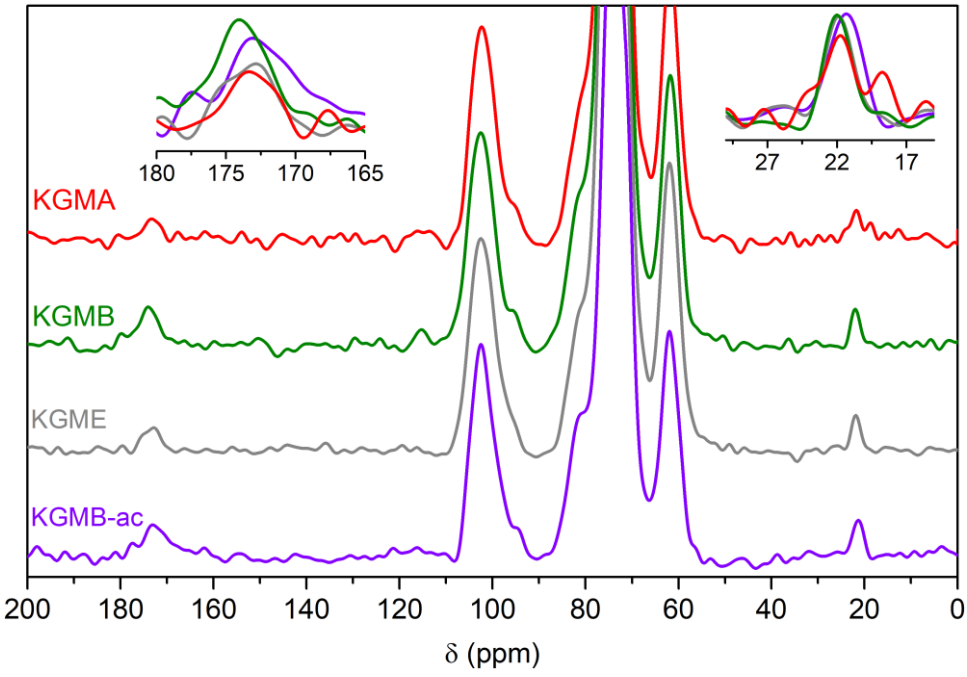

Figure 5: ^{13}C SPE-MAS spectra of selected KGM samples (quantitative for all signals except possibly the carbonyl signal at 173 ppm, normalized to signal D at 103 ppm).

3.4. Comparison of solid-state spectroscopy methods

To assess the potential calibration of DA_{CP} and DA_{IR}, their relationship with the quantitative $DA_{SPE,q}$ values was examined. $DA_{SPE,q}$ against DA_{CP} exhibited a fair linear fit (Figure 6a), with a R^2 value of 0.6 reflecting the relatively large error bars of $DA_{SPE,q}$ values. This fair fit

indicated that the DA_{CP} values were, as expected, on an arbitrary scale, which can be calibrated through a correction factor. The slope of the linear fit of $DA_{SPE,q}$ against DA_{CP} was thus used as a correcting factor for the DA_{CP} values using Eq. 4. This calibrates the DA_{CP} values by converting them to the same scale as the quantitative ^{13}C SPE-MAS measurements. Furthermore, the *RSD* of the resulting quantitative $DA_{CP,q}$ values was calculated with Eq. 5, determined from error calculations taking into account the errors on DA_{CP} and on the correcting factor (slope). The corrected values are given in Table S8 for all samples.

$$DA_{CP,q} = DA_{CP} \cdot (0.936 \pm 0.063) \quad (4)$$

$$RSD_{DA_{CP,q}} = DA_{CP} \cdot \sqrt{\left(\frac{RSD_{DA_{CP}}}{DA_{CP}}\right)^2 + \left(\frac{0.063}{0.936^2}\right)^2} \quad (5)$$

$DA_{SPE,q}$ against DA_{IR} exhibited no linear fit (Figure 6b), as indicated by a negative R^2 value. Thus, the DA_{IR} values could not be corrected through a simple correction factor.

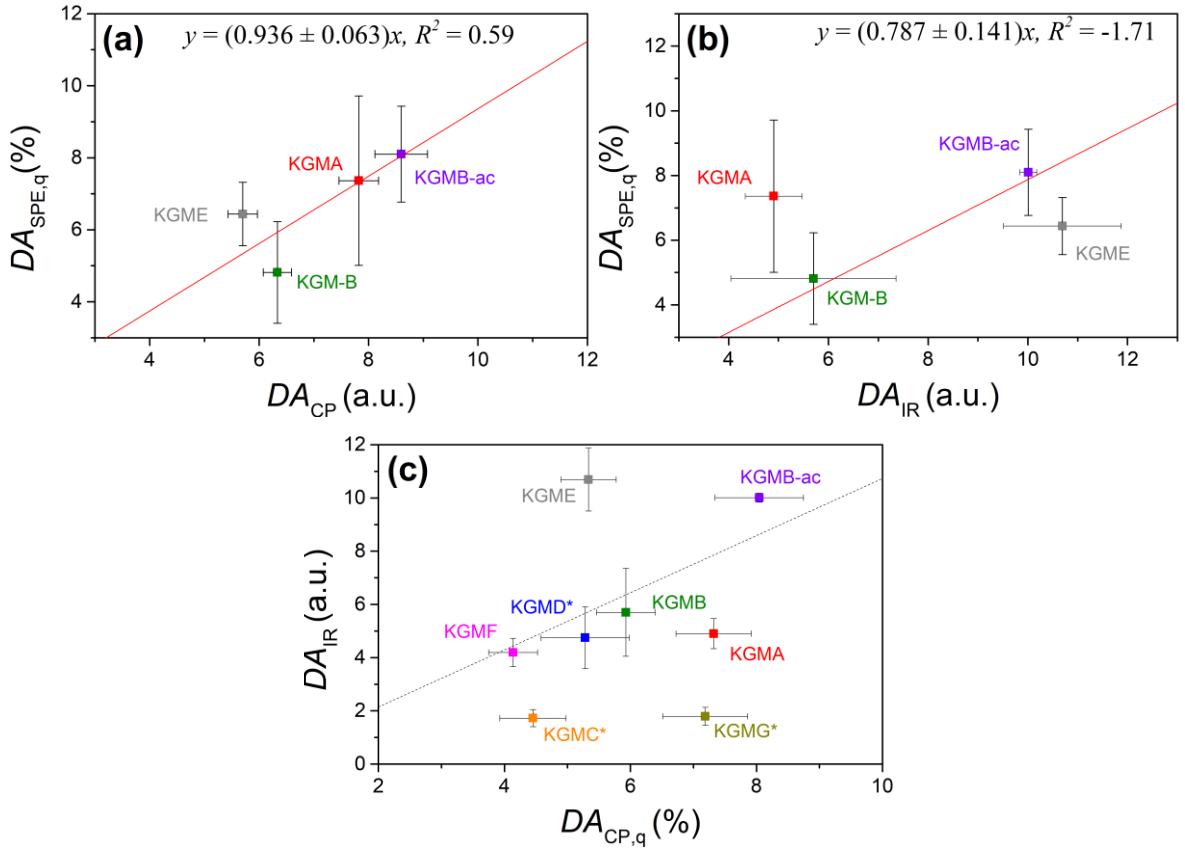

Figure 6: DA values of KGM samples determined from different methods. (a) $DA_{SPE,q}$ against *DA_{CP}, (b) $DA_{SPE,q}$* against *DA_{IR}, with their linear fits (solid lines). (c) DA_{IR}* against *$DA_{CP,q}$, with*

*impure samples labelled with an *, and the linear fit of the pure samples data shown as a guide to the eye (dotted line, see Figure S20 for the fit).*

For *DA* values determined by ^{13}C NMR, DA_{CP} values (determined by semi-quantitative CP-MAS) were more precise (as shown by their smaller *RSD*s), while $DA_{SPE,q}$ values (determined by quantitative SPE-MAS) were more accurate (Gaborieau et al., 2010). The corrected $DA_{CP,q}$ values combined accuracy and better precision, and were the NMR-determined values selected for the comparison with FTIR-determined values. The DA_{IR} values were plotted against the $DA_{CP,q}$ values for comparison (Figure 6c), with the line of best fit of the pure samples shown. $DA_{CP,q}$ values showed that acetylation ranged from 4 to 8 % of hexoses in all samples (except KGMB-ac), in broad agreement with published studies (Alonso-Sande et al., 2009; Chua et al., 2012; Williams et al., 2000). $DA_{CP,q}$ values also showed that the acetylation reaction on KGMB increased its *DA* by 15 to 60 %. KGMA, KGMG and KGMB-ac were significantly more acetylated than the other samples. KGMB was significantly more acetylated than KGMC and KGMF.

DA_{IR} values did not follow the same trend as $DA_{CP,q}$ values (Figure 6c), with strong deviations for KGME, KGMC and KGMG. Excipients (including magnesium stearate) did not explain these deviations, as KGME does not contain excipients and did not follow the trend. The deviations may be explained by the limited penetration depth of the infrared irradiation (about 2 μm (Sevenou et al., 2002)). ATR-FTIR thus yielded a biased measurement of *DA*, as only the outer layer of the KGM particles was measured. This allowed a qualitative assessment of the homogeneity of acetylation throughout the particles. Comparatively higher DA_{IR} values for KGME and KGMB-ac indicated higher acetylation in the outer layers of the particles than in their central parts. This is consistent with acetylating KGMB into KGMB-ac in a solvent that does not fully dissolve the KGM particles and leads to preferential acetylation in the outer layers of the particles. On the other hand, comparatively lower DA_{IR} values for KGMA, KGMC and KGMG indicate lower acetylation in the outer layers of the particles than in their central parts. In an earlier study, acetylation was measured in the same product KGMA (named NKF) with an established titrimetric method and was found to be 2 % w/w of acetyl-substituted residues in the KGM backbone (Chua et al., 2012), which corresponds to a *DA* of 8.1 % of the hexoses (Gao & Nishinari, 2004); this is in broad agreement with the $DA_{CP,q}$ value, but not the DA_{IR} value, determined in the present work.

4. Conclusions

Common aqueous and organic solvents did not allow complete molecular solubility of selected KGM samples, yielding at best fine dispersions. A meaningful characterization of whole KGM samples in solution is not possible until KGM forms a true solution. Other avenues should be explored to fully dissolve KGM, with ionic liquids as potential alternative solvents already used for starch or cellulose and tested for glucomannans (El Seoud et al., 2007). Transparency is necessary but not sufficient for complete molecular solubility, and KGM's molecular solubility in transparent dispersions should be quantified, for example with solution-state NMR as done previously for starch (Schmitz et al., 2009) or poly(acrylic acid) (Maniego et al., 2017). Obtaining a true solution would open the way to the homogeneous chemical functionalization of KGM, and to the characterization of its molecular structure, for example of its sizes with size-exclusion chromatography, of its average composition by solution-state NMR, chromatography or capillary electrophoresis, or of their heterogeneity at the molecular level by separation techniques (e.g., chromatography, capillary electrophoresis) (Thevarajah et al., 2016b).

The critical assessment of different methods for KGM dissolution and for *DA* determination leads us to recommend the use of solid-state methods for *DA* determination to avoid bias due to incomplete dissolution. Solid-state spectroscopic methods were chosen and developed in this work to assess the degree of acetylation in KGM. Fast ATR-FTIR enabled a qualitative assessment of acetylation, which is selective to the outer layer of KGM particles, and identifying excipients like magnesium stearate. Thus, this method is recommended for qualitative (structure elucidation) but not quantitative (*DA* determination) sample analysis.

Solid-state ^{13}C NMR allowed a meaningful quantification of the average degree of acetylation *DA* in KGM. Semi-quantitative measurements by ^{13}C CP-MAS NMR allowed the comparison of samples on the same arbitrary scale; the precision of the measurement was assessed from the *SNR* of the methyl acetyl group. The calibration (with longer ^{13}C SPE-MAS NMR measurements) of the arbitrary scale of the *DA* values from ^{13}C CP-MAS provided quantitative *DA* values for selected KGM samples, ranging from 4 to 8 % of the hexoses in the KGM backbone, in agreement with previously reported values. The present study provided the first meaningful quantification of *DA* in KGM in the solid state. It opens the way to the quantification of acetylation in a broader range of KGM samples. This analytical procedure

can be applied to characterize the pharmaceutical grade of KGM and could be adopted by regulatory authorities as a pharmacopoeia standard. Most analyses of food-grade KGM currently depend on back-titration of glucose after complete hydrolysis of the given KGM powder (Chua et., 2010). The proposed *DA* quantification methodology by solid-state NMR will provide better quality control of KGM, and support, for example, studies of the role of acetylation in functional properties like processing (e.g., gelation) of glucomannan and glucomannan acetate samples with a broader range of *DA* values, or KGM nutritional and health benefits.

Declaration of Competing Interest

None.

Acknowledgments

The authors acknowledge the Advanced Materials Characterisation Facility (AMCF) of Western Sydney University for access to instrumentation and help from staff, some suppliers for KGM research samples, Wayne Higginbotham and Paul Roddy for assistance in acetylation reactions. This research did not receive any specific grant from funding agencies in the public, commercial, or not-for-profit sectors.

References

Alonso-Sande, M., Teijeiro-Osorio, D., Remunan-Lopez, C., & Alonso, M. J. (2009). Glucomannan, a promising polysaccharide for biopharmaceutical purposes. *Eur. J. Pharm. Biopharm., 72*, 453-462.

Brigden, C. J., & Wilkinson, S. G. (1985). Structural studies of acidic glucomannans from strains of Serratia marcescens O14 and O6. *Carbohydr. Polym., 138*, 267-276.

Castignolles, P., Graf, R., Parkinson, M., Wilhelm, M., & Gaborieau, M. (2009). Detection and quantification of branching in polyacrylates by size-exclusion chromatography (SEC) and melt-state 13C NMR spectroscopy. *Polymer, 50*, 2373-2383.

Chua, M., Baldwin, T. C., Hocking, T. J., & Chan, K. (2010). Traditional uses and potential health benefits of Amorphophallus konjac K. Koch ex N.E.Br. *J. Ethnopharmacol., 128*, 268-278.

Chua, M., Chan, K., Hocking, T. J., Williams, P. A., Perry, C. J., & Baldwin, T. C. (2012). Methodologies for the extraction and analysis of konjac glucomannan from corms of Amorphophallus konjac K. Koch. *Carbohydr. Polym., 87*, 2202-2210.

Du, X., Li, J., Chen, J., & Li, B. (2012). Effect of degree of deacetylation on physicochemical and gelation properties of konjac glucomannan. *Food Res. Int., 46*, 270-278.

El Seoud, O. A., Koschella, A., Fidale, L. C., Dorn, S., & Heinze, T. (2007). Applications of ionic liquids in carbohydrate chemistry: A window of opportunities. *Biomacromolecules, 8*, 2629-2647.

Felix da Silva, D., Ogawa, C. Y. L., Sato, F., Neto, A. M., Larsen, F. H., & Matumoto-Pintro, P. T. (2020). Chemical and physical characterization of konjac glucomannan-based powders by FTIR and 13C MAS NMR. *Powder Technol., 361*, 610-616.

Furuhata, K. I., Koganei, K., Chang, H. S., Aoki, N., & Sakamoto, M. (1992). Dissolution of cellulose in lithium bromide organic-solvent systems and homogeneous bromination of cellulose with N-bromosuccinimide triphenylphosphine in lithium bromide N,N-dimethylacetamide. *Carbohydr. Res., 230*, 165-177.

Gaborieau, M., & Castignolles, P. (2011). Size-exclusion chromatography (SEC) of branched polymers and polysaccharides. *Anal. Bioanal. Chem., 399*, 1413-1423.

Gaborieau, M., Nebhani, L., Graf, R., Barner, L., & Barner-Kowollik, C. (2010). Accessing quantitative degrees of functionalization on solid substrates via solid-state NMR spectroscopy. *Macromolecules, 43*, 3868-3875.

Gao, S. J., & Nishinari, K. (2004). Effect of degree of acetylation on gelation of konjac glucomannan. *Biomacromolecules, 5*, 175-185.

Gidley, M. J., McArthur, A. J., & Underwood, D. R. (1991). 13C NMR characterization of molecular structures in powders, hydrates and gels of galactomannans and glucomannans. *Food Hydrocoll., 5*, 129-140.

Gomes Neto, R. J., Genevro, G. M., Paulo, L. D. A., Lopes, P. S., de Moraes, M. A., & Beppu, M. M. (2019). Characterization and in vitro evaluation of chitosan/konjac glucomannan bilayer film as a wound dressing. *Carbohydr. Polym., 212*, 59-66.

Huang, L., Takahashi, R., Kobayashi, S., Kawase, T., & Nishinari, K. (2002). Gelation behavior of native and acetylated konjac glucomannan. *Biomacromolecules, 3*, 1296-1303.

Kato, K., & Matsuda, K. (1969). Studies on the chemical structure of konjac mannan. *Agric. Biol. Chem., 33*, 1446-1453.

Katsuraya, K., Okuyama, K., Hatanaka, K., Oshima, R., Sato, T., & Matsuzaki, K. (2003). Constitution of konjac glucomannan: chemical analysis and 13C NMR spectroscopy. *Carbohydr. Polym., 53*, 183-189.

Keithley, J., & Swanson, B. (2005). Glucomannan and obesity: a critical review. *Altern. Ther. Health Med., 11*, 30.

Kok, M. S., Abdelhameed, A. S., Ang, S., Morris, G. A., & Harding, S. E. (2009). A novel global hydrodynamic analysis of the molecular flexibility of the dietary fibre polysaccharide konjac glucomannan. *Food Hydrocolloids, 23*, 1910-1917.

Koroskenyi, B., & McCarthy, S. P. (2001). Synthesis of acetylated konjac glucomannan and effect of degree of acetylation on water absorbency. *Biomacromolecules, 2*, 824-826.

Kruk, J., Kaczmarczyk, K., Ptaszek, A., Goik, U., & Ptaszek, P. (2017). The effect of temperature on the colligative properties of food-grade konjac gum in water solutions. *Carbohydr. Polym., 174*, 456-463.

Maniego, A. R., Sutton, A. T., Gaborieau, M., & Castignolles, P. (2017). Assessment of the branching quantification in poly(acrylic acid): Is it as easy as it seems? *Macromolecules, 50*, 9032-9041.

Morcombe, C. R., & Zilm, K. W. (2003). Chemical shift referencing in MAS solid state NMR. *J. Magn. Reson., 162*, 479-486.

Nishinari, K. (2000). Konjac glucomannan. *Dev. Food Sci., 41*, 309-330.

Nishinari, K., Williams, P., & Phillips, G. (1992). Review of the physico-chemical characteristics and properties of konjac mannan. *Food hydrocoll., 6*, 199-222.

Ratcliffe, I., Williams, P. A., Viebke, C., & Meadows, J. (2005). Physicochemical characterization of konjac glucomannan. *Biomacromolecules, 6*, 1977-1986.

Rebiere, J., Heuls, M., Castignolles, P., Gaborieau, M., Rouilly, A., Violleau, F., & Durrieu, V. (2016). Structural modifications of cellulose samples after dissolution into various solvent systems. *Anal. Bioanal. Chem., 408*, 8403-8414.

Rinaudo, M. (2006). Characterization and properties of some polysaccharides used as biomaterials. *Macromol. Biosci., 245-246*, 549-557.

Schmitz, S., Dona, A. C., Castignolles, P., Gilbert, R. G., & Gaborieau, M. (2009). Assessment of the extent of starch dissolution in dimethyl sulfoxide by 1H NMR spectroscopy. *Macromol. Biosci., 9*, 506-514.

Sevenou, O., Hill, S. E., Farhat, I. A., & Mitchell, J. R. (2002). Organisation of the external region of the starch granule as determined by infrared spectroscopy. *Int. J. Biol. Macromol., 31*, 79-85.

Singh, S., Singh, G., & Arya, S. K. (2018). Mannans: An overview of properties and application in food products. *Int. J. Biol. Macromol., 119*, 79-95.

Spiess, H. W. (2017). 50th anniversary perspective: The importance of NMR spectroscopy to macromolecular science. *Macromolecules, 50*, 1761-1777.

Stephen, A. M., & Churms, S. C. (2006). Introduction. In A. M. Stephen, G. O. Phillips & P. A. Williams (Eds.). *Food polysaccharides and their applications* (pp. 1-24). Boca Raton: CRC Taylor & Francis.

Thevarajah, J. J., Bulanadi, J. C., Wagner, M., Gaborieau, M., & Castignolles, P. (2016a). Towards a less biased dissolution of chitosan. *Anal. Chim. Acta, 955*, 258-268.

Thevarajah, J. J., Sutton, A. T., Maniego, A. R., Whitty, E. G., Harrisson, S., Cottet, H., Castignolles, P., & Gaborieau, M. (2016b). Quantifying the heterogeneity of chemical structures in complex charged polymers through the dispersity of their distributions of electrophoretic mobilities or of compositions. *Anal. Chem., 88*, 1674-1681.

Vieira, M., & Gil, A. (2005). A solid state NMR study of locust bean gum galactomannan and konjac glucomannan gels. *Carbohydr. Polym., 60*, 439-448.

Williams, M. A. K., Foster, T. J., Martin, D. R., Norton, I. T., Yoshimura, M., & Nishinari, K. (2000). A molecular description of the gelation mechanism of konjac mannan. *Biomacromolecules, 1*, 440-450.

Wu, C., Peng, S., Wen, C., Wang, X., Fan, L., Deng, R., & Pang, J. (2012). Structural characterization and properties of konjac glucomannan/curdlan blend films. *Carbohydr. Polym., 89*, 497-503.

Yang, G., Xiong, X. P., & Zhang, L. (2002). Microporous formation of blend membranes from cellulose/konjac glucomannan in NaOH/thiourea aqueous solution. *J. Memb. Sci., 201*, 161-173.

Zhang, Y.-Q., Xie, B.-J., & Gan, X. (2005). Advance in the applications of konjac glucomannan and its derivatives. *Carbohydr. Polym., 60*, 27-31.

Zhu, F. (2018). Modifications of konjac glucomannan for diverse applications. *Food Chem., 256*, 419-426.

Supplementary material for

Assessing the Quantification of Acetylation in Konjac Glucomannan via FTIR and Solid-state NMR Spectroscopy

Kash A. Bhullar [a], *Michael I. M. Horgan* [a], *Ashley Le* [a], *David Fania* [b], *Richard Wuhrer* [b], *Valentina Razmovsi-Naumovski* [c,d], *Kelvin Chan* [c,e], *Patrice Castignolles* [a,f] *Marianne Gaborieau*[a]

[a] Western Sydney University, Australian Centre for Research On Separation Science (ACROSS), School of Science, Parramatta Campus, Locked Bag 1797, Penrith NSW 2751, Australia

[b] Western Sydney University, Advanced Materials Characterisation Facility, Parramatta Campus, Locked Bag 1797, Penrith NSW 2751, Australia

[c] Western Sydney University, NICM Health Research Institute, School of Science, Campbelltown campus, Locked Bag 1797, Penrith NSW 2751, Australia

[d] South West Sydney Clinical Campuses, Discipline of Medicine, University of New South Wales Sydney, NSW 2170, Australia

[e] Liverpool John Moores University, School of Pharmacy & Biomolecular Sciences, Liverpool L3 3AF, United Kingdom

[f] Sorbonne University, Parisian Institute of Molecular Chemistry, UMR 8232, Polymer Chemistry team, 75252 Paris, France

Visual observation of dissolution

The dissolution of a polysaccharide depends on its structure. KGM is branched and partially acetylated. Acetylation and branching lead to irregular molecular structure, which prevents the regular packing of polysaccharide chains; this comparatively increases solubility and disassociation of the molecular chains for KGM compared to the corresponding linear, non-substituted polysaccharide cellulose (linear homopolymer of D-glucose with β(1,4) linkages) (Du, Li, Chen & Li, 2012; Kok, Abdelhameed, Ang, Morris & Harding, 2009; Williams et al., 2000).

The selection of a container (vial) and its surface to carry out dissolution can play a significant role in solubility. For example, it is known from basic chemistry that scratching the surface of a glass container accelerates sample precipitation due to the increase in surface area for nucleation to occur. The material (glass, plastic, etc.) and geometry of the surface (i.e., sharp bottom in Figures S1A-B, flat bottom in Figures S1C-D) is an important but often overlooked feature of solubility studies.

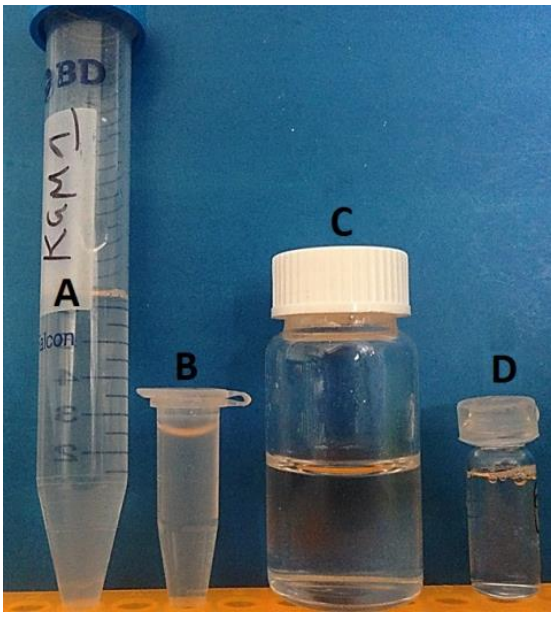

Figure S1: Dissolution of KGMA in Milli-Q water as given in table 5 in different containers. A) 10 mL plastic tube, B) 2 mL plastic tube, C) 20 mL glass vial and D) 2 mL glass vial.

The effect of the vial surface on solubility was demonstrated on starch dissolution.(Hernandez et al., 2008) Nucleation was initiated by edges of a vial surface in flat-based glass vials. A change in the vial geometry to a round bottom to lessen potential nucleation on surface edges was effective in reducing the precipitation in further starch solubility studies. The compatibility

of the container and solvent should also be factored into solubility studies. Organic solvents are incompatible with plastic vials due to reactions that may occur between the solvent and constituents of the plastic vial and to possible leaching of the polymer or its additives into the solvent.(McDonald et al., 2008; Mori, 1979) Glass containers (with flat base) are recommended for organic solvents since these do not react with glass. For aqueous solvents, the dominant constituent is water, and since plastics are predominantly hydrophobic, no side reactions or leaching are expected to occur in solution. A potential issue with glass vials and aqueous solvents is that at very high pH these solvents etch the glass. Thus, glass vials are not suitable for aqueous solutions of high pH. The surface geometry and material of the container thus play a very important role. To determine the best container for the solubility studies replicate dissolutions of KGMA at 0.5 $g.L^{-1}$ in Milli-Q water at 80°C were carried out in containers of different sizes, materials and geometries (Table S1).

Table S1: Visual observation of KGMA dissolution at 0.5 $g.L^{-1}$ in MQ water at 80 °C in different containers (T = Turbid, P = Particles).

Observation	Containers			
	Plastic		Glass	
	15-mL sharp-bottom tube, *Figure 2A*	2-mL sharp-bottom tube, *Figure 2B*	15-mL flat-bottom vial, *Figure 2C*	2-mL flat-bottom vial, *Figure 2D*
Before heating	T	T	T	T
After 3 h	T	T	T	T
After 24 h	P	P	P	P
After 48 h	P	P	P	P

Table S2: Detailed description of visual description designations.

Designation	Description
Particles (P)	Aggregates visible in solution
Clear solution (C)	Complete dissolution visually
Almost clear solution (*C)	Incomplete dissolution visually
Turbid (T)	Fine particles present making the solution slightly opaque
Did not dissolve (D)	Sample visually not dissolving at all
Not carried out (n.c.)	Solubility experiment was not carried out

Table S3: Visual observations of solubility at different nominal concentrations after 3 h at 80 °C in aqueous solvents (Glu = glucose, SS = soluble starch, percentages are weight/weight, see Table S2 for details of visual observation codes). Water is of Milli-Q quality.

Solvent	Conc. ($g.L^{-1}$)	Sample								
		Glu	SS	KGM						
				A	B	C	D	E	F	S
Water	0.625	C	C	P	P	P	P	n.c.	n.c.	D
	0.5	C	C	*C	*C	P	P	P	P	n.c.
	0.1	C	C	T	T	T	T	P	T	n.c.
Water with 5 % NaCl	0.1	C	C	T	T	T	T	P	T	n.c.
Water with 98 % NaCl	0.5	C	C	P	P	P	P	P	P	n.c.
Water with 0.01 M NaOH	0.625	C	C	*C	*C	T	T	P	P	n.c.
Water with 0.1 M NaOH	0.5	n.c.	C	*C	n.c.	n.c.	n.c.	n.c.	n.c.	n.c.

Table S4: Visual observations of solubility at different nominal concentrations after 3 h at 80 °C in organic solvents (Glu = glucose, SS = soluble starch, percentages are weight/weight, see Table S2 for details of visual observation codes).

Solvent	Conc. ($g.L^{-1}$)	Sample								
		Glu	SS	KGM						
				A	B	C	D	E	F	S
DMSO (non-anhydrous)	0.625	C	C	P	P	P	P	n.c.	n.c.	D
	0.5	C	C	T	T	T	T	T	P	n.c.
DMSO (non-anhydrous) with 98 % LiBr	0.625	C	C	T	T	T	T	n.c.	n.c.	D
	0.5	C	C	T	T	T	T	T	P	n.c.
DMSO (anhydrous)	0.5	C	C	T	T	P	P	P	P	n.c.
	0.1	C	C	T	T	T	T	T	T	n.c.
DMSO (anhydrous) with 5 % LiBr	0.1	C	P	T	T	T	T	T	T	n.c.
DMSO (anhydrous) with 98 % LiBr	0.1	C	T	T	T	T	T	T	T	n.c.
DMAc (non-anhydrous)	0.5	C	T	T	T	T	T	T	T	n.c.
	0.1	C	*C	T	T	T	T	T	T	n.c.
DMAc (non-anhydrous) with 5 % LiBr	0.1	C	*C	T	T	P	P	P	P	n.c.

FTIR spectroscopy

Signal assignment

Table S5: Signal assignment for ATR-FTIR spectra of KGM samples in the 4000 - 600 cm^{-1} range (see Figure 2 for spectra and labels). Key for modes: δ bending, ν stretching, ρ rocking, s symmetric, as antisymmetric; key for intensities: w weak, m medium, s strong, vs very strong. Experimental peak assignment is compared to information published for KGM in in references 1 (Xu et al., 2008), 2 (Liu, Fan, Wang & He, 2007), 3 (Chua et al., 2012), and 5 (Yu, Huang, Ying & Xiao, 2007), and for magnesium stearate in reference 4 (Nep & Conway, 2012).

Label	Wavenumber (cm^{-1})	Assignment	Comment	KGM sample								Ref.			
				A	B	C	D	E	F	G	B-ac	1	2	3	4
A	~3350	ν(O-H)	intermolecularly bonded	m	m	m	m	m	m	m	w	vs	s	m	w
B, C	2920, 2850	ν_{as}(C-H), ν_{s}(C-H)	broad	w	w	w	w	m	w	w	w	m	w	w	
			sharp, magnesium stearate			w	m			s					s
D	1730	ν(C=O)	ester (acetyl group)	w	w	w	w	m	w	w	w	m	w	w	
E	1635	δ(HOH)	water in KGM (ref. 5)	m	m	m	m	m	m	m	m	s	m	m	
F	1580	$\delta_{as}(COO^{-})$	magnesium stearate			w	w			m					s
G	1540	$\delta_{as}(CH_3)$	hydroxypropyl methylcellulose?							m					m
H	1465	$\delta_{s}(CH_2)$	magnesium stearate			w	w			m					s
I	1425	$\delta_{s}(CH_2)$		m	m	m	m	m	m	m	m	m	w		
J	1375	δ_{s}(CH)		m	m	m	m	m	m	m	m	w	w	m	
K	1315	δ(CH)		w	w	w	w	w	w	w	w	w	m	w	
L	1240	ν(C-O)	ester (acetyl group)	m	m	w	m	m	m	m	w	w		w	
M	1150	ν(C-O)	ether	w	w	w	w	w	w	w	w	m	m	w	
N	1110	ν(C-O)	ether (starch?)							w					
O	1075-1060	δ(CH)		w	w	w	w	w	w	w	w	s	s	m	
P	1015	ν(C-O-C)	pyranose ring	vs	vs	vs	vs	vs	vs	vs		vs	s	vs	
Q	940	$\rho(CH_3)$		w	w	w	w	w	w	w		w	w		
R, S	895, 865	δ(C-O-C)	β-mannosidic linkage	w	w	w	w	w	w	w	w	w	w	m	
T	805	δ(C-O-C)	β-mannosidic linkage	m	m	w	m	m	m	w	m	m	m	m	
U	750	$\rho(CH_2)$	glucose, magnesium stearate	w	w	w	w	w	w	w	w	m	w		w
V	670	$\nu(CH_2)$	starch?			w									

FTIR method development

ATR-FTIR spectra of samples KGMA to KGMF were recorded for comparison with a 2 cm^{-1} resolution, with 32 scans using a PerkinElmer Spectrum 100 FTIR instrument with a diamond ATR window crystal, the data treated and normalized using the PerkinElmer Spectrum 6.3.5 software (Figure S2). They were compared to spectra recorded on the Bruker Vertex 7-0 spectrometer (Figure 2). Subsequent ATR-FTIR spectra were all recorded on the spectrometer providing the best sensitivity and resolution for the acetyl band at 1730 cm^{-1} (labelled D in Figure 2), the Bruker Vertex 70.

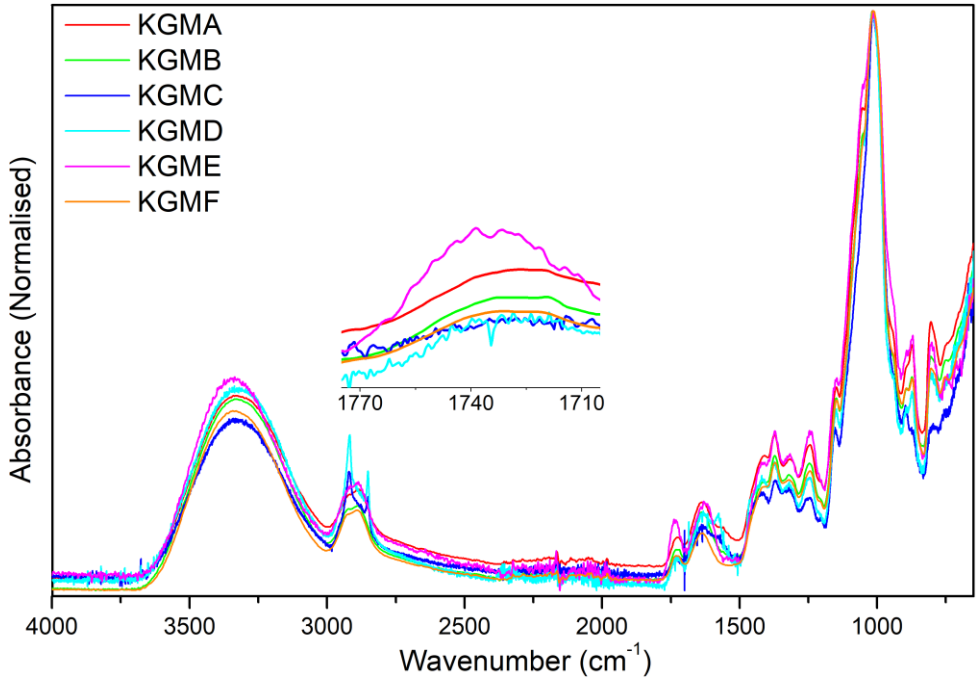

Figure S2: ATR-FTIR spectra of KGM powder samples (PerkinElmer spectrometer).

The accuracy of ATR-FTIR spectra may be affected by the limited penetration depth of the irradiation in the sample (about 2 μm (Sevenou, Hill, Farhat & Mitchell, 2002)), transmission FTIR spectra of KGM samples in KBr pellets were thus acquired to try and overcome this limitation. For transmission FTIR, KBr pellets were prepared with 2 (w/w) % KGM and kept in desiccators overnight to stabilize the moisture content. Transmission FTIR spectra however exhibited a very limited resolution of the band at 1730 cm^{-1}, even after storage of the KBr pellets in a desiccator to limit or control the water content of KGM (Figures S3 and S4), and was not further pursued.

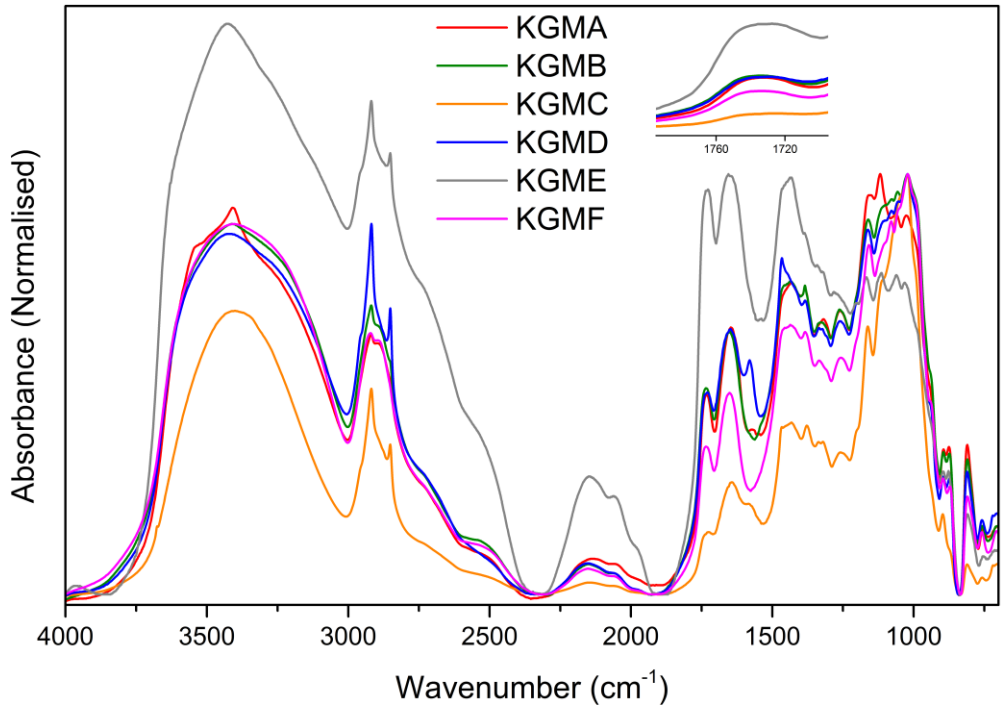

Figure S3: Transmission FTIR spectra of non-desiccated KBr pellets of KGM samples (PerkinElmer spectrometer).

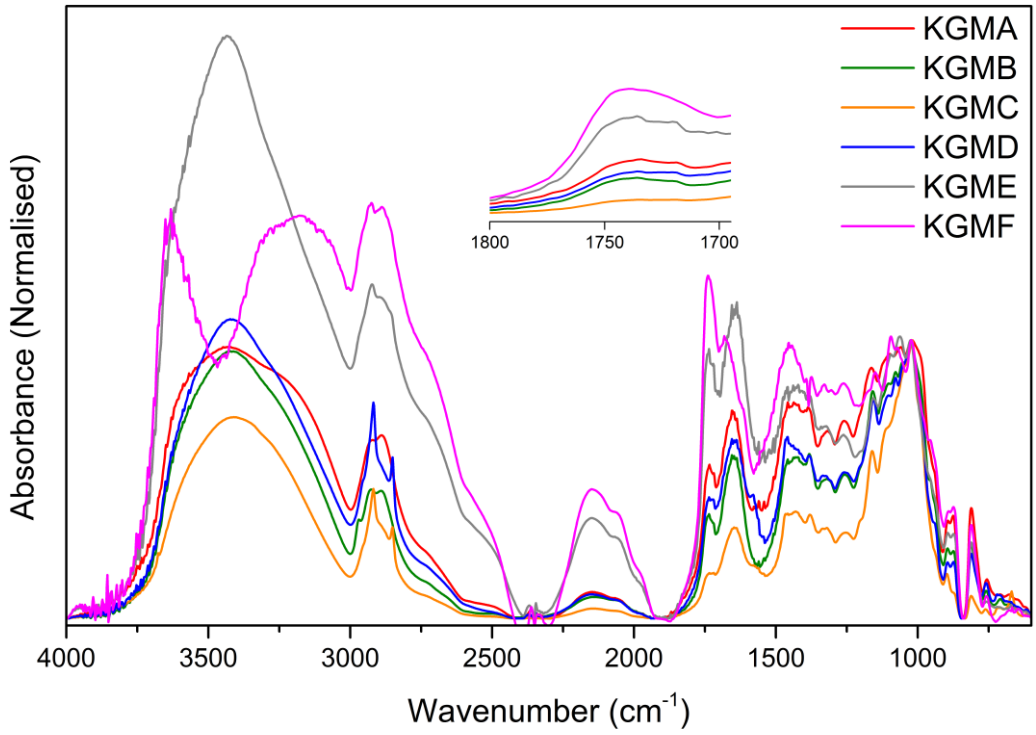

Figure S4: Transmission FTIR spectra of desiccated KBr pellets of KGM samples (Bruker spectrometer).

ATR-FTIR data treatment was examined in terms of the effects of ATR-FTIR correction, line smoothing, and number of iterations for baseline correction on OPUS software (with sample KGMA, Figure S5). The acetyl band of interest at 1730 cm^{-1} is more resolved with ATR correction. Smoothing over 25 points did not significantly affect the bands of interest. 51 iterations of baseline correction yielded a higher resolution than 1 to 41 iterations for the acetyl band of interest at 1730 cm^{-1}.

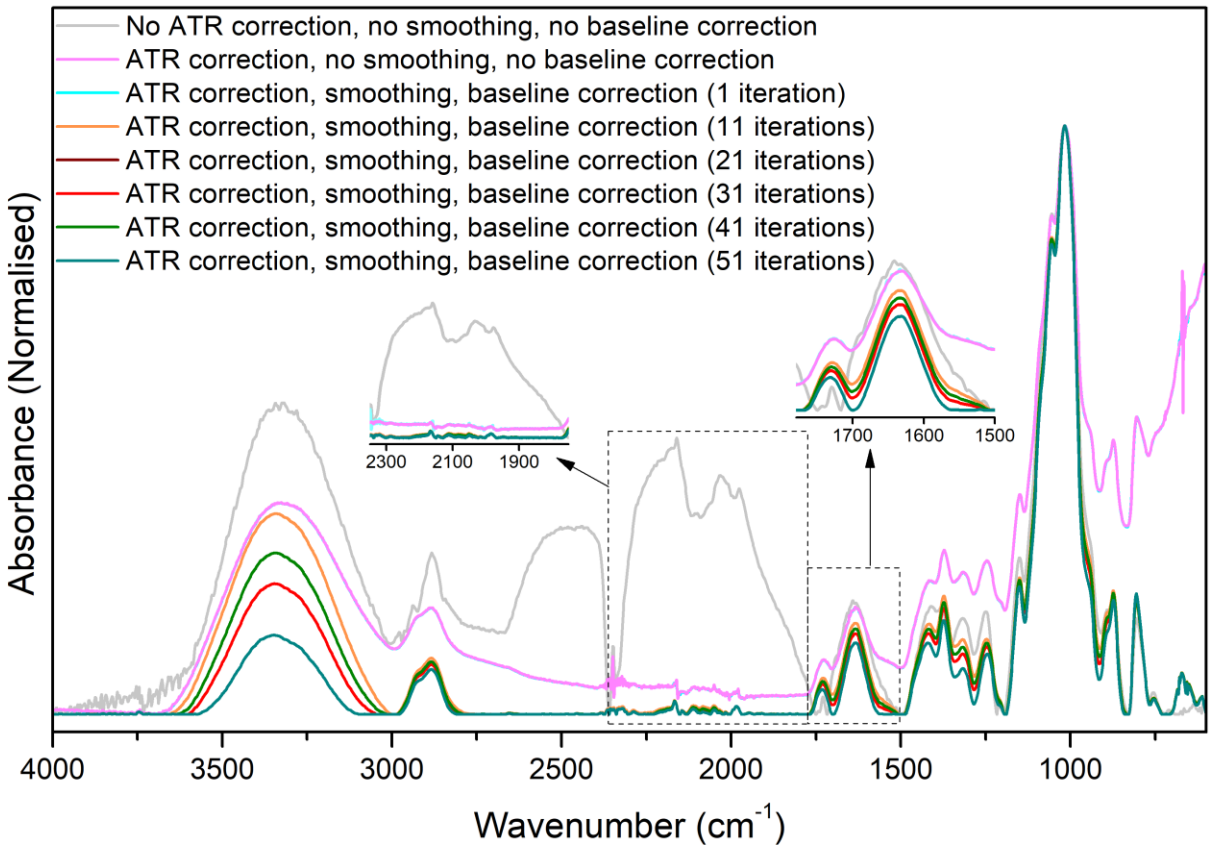

Figure S5: ATR-FTIR spectra (Bruker spectrometer) of KGMA with different data treatment.

Replicate ATR FTIR spectra

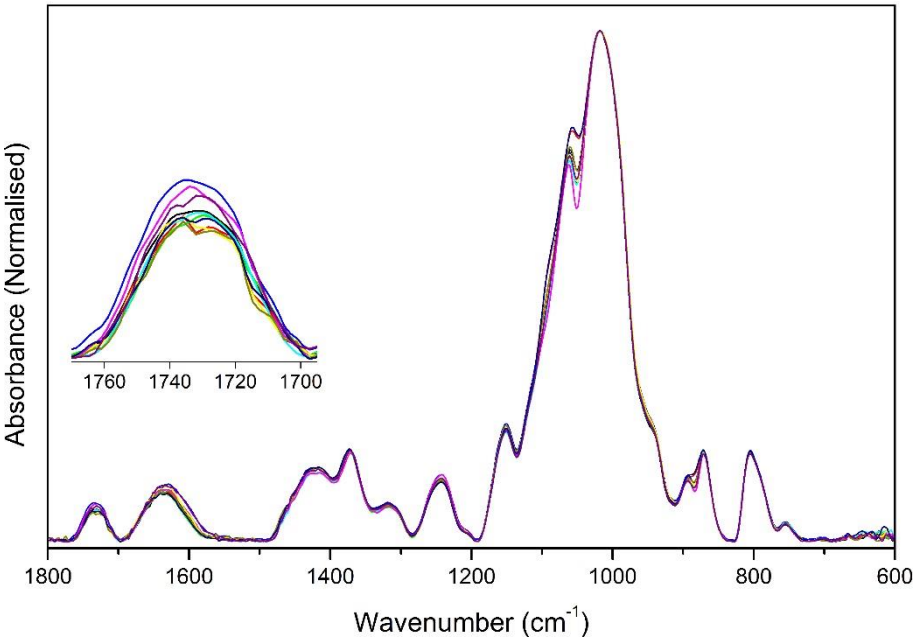

Figure S6: 10 replicate ATR-FTIR spectra of KGMA.

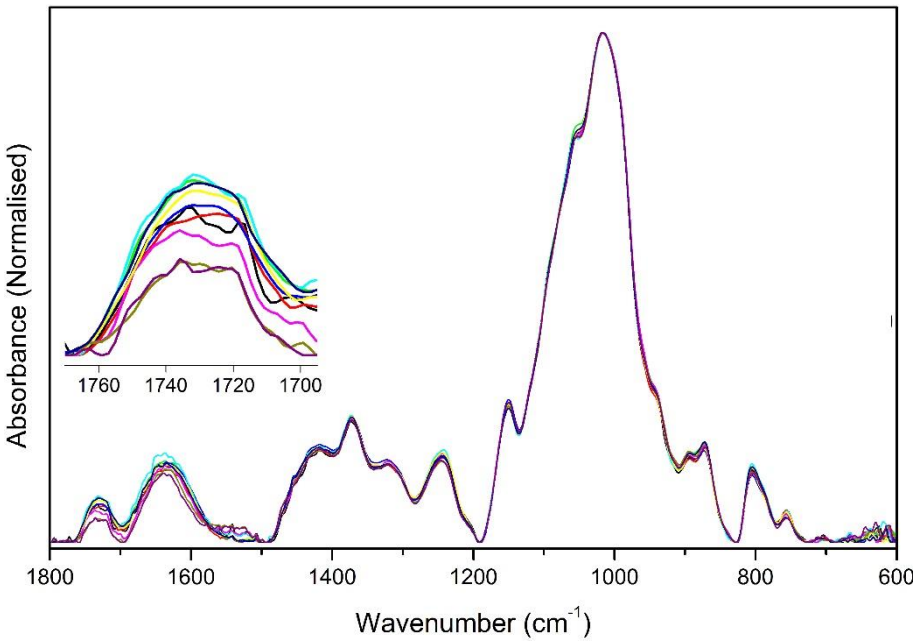

Figure S7: 10 replicate ATR-FTIR spectra of KGMB.

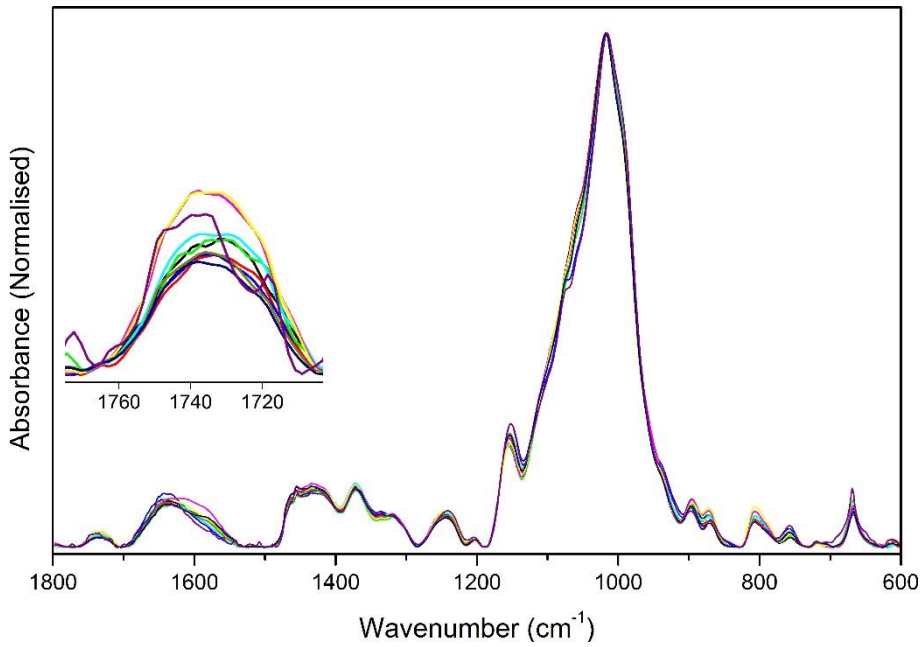

Figure S8: 10 replicate ATR-FTIR spectra of KGMC.

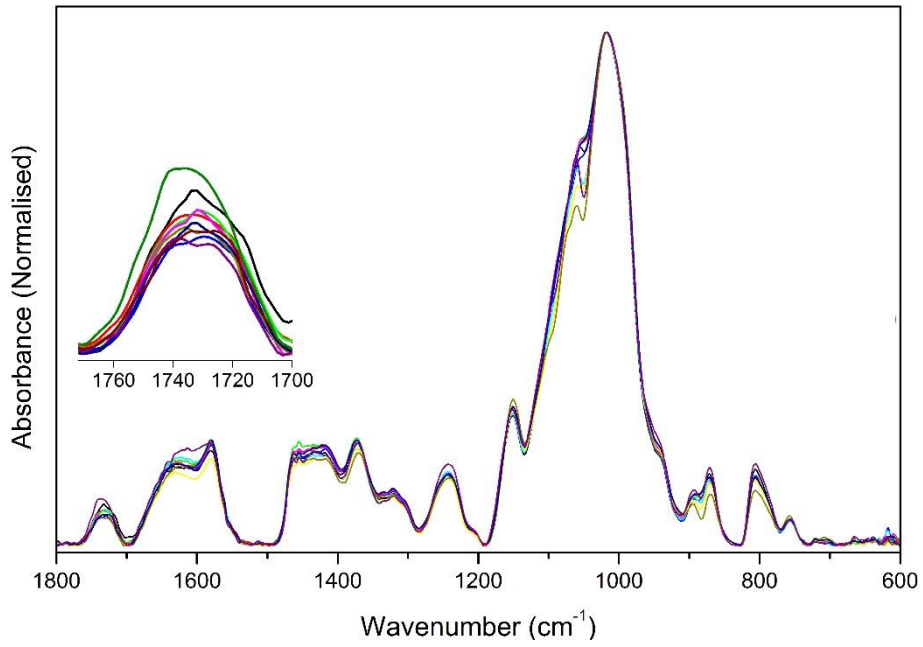

Figure S9: 10 replicate ATR-FTIR spectra of KGMD.

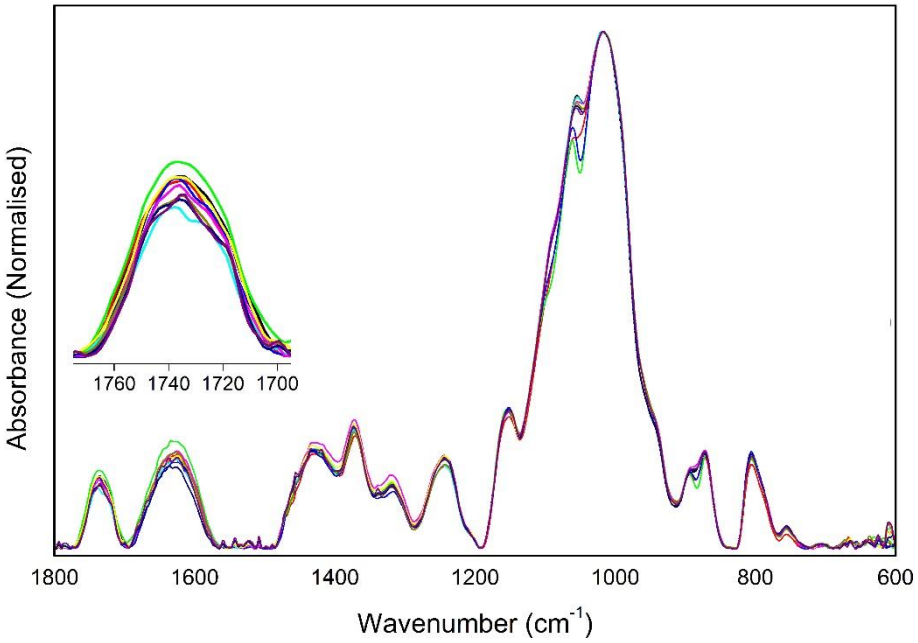

Figure S10: 10 replicate ATR-FTIR spectra of KGME.

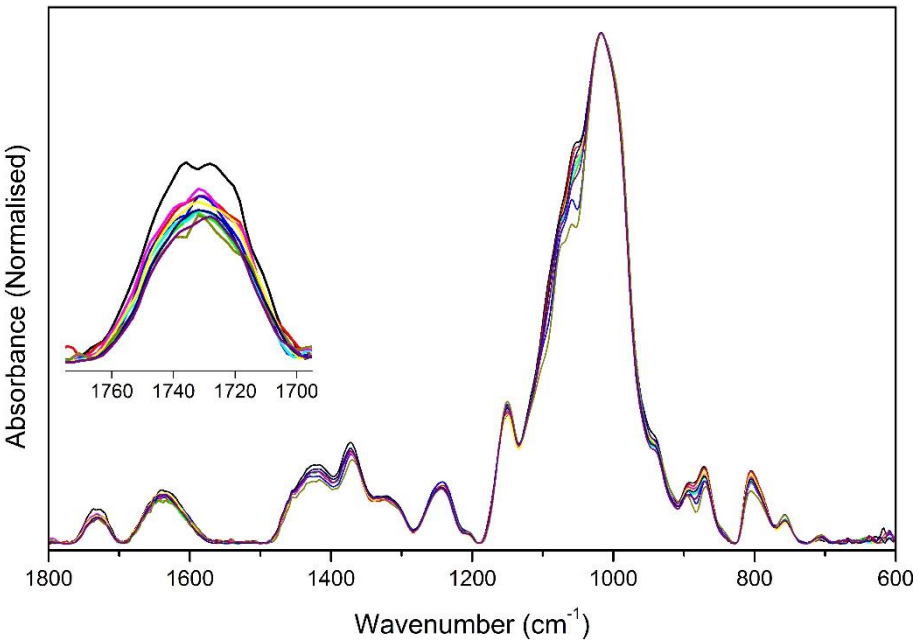

Figure S11: 10 replicate ATR-FTIR spectra of KGMF.

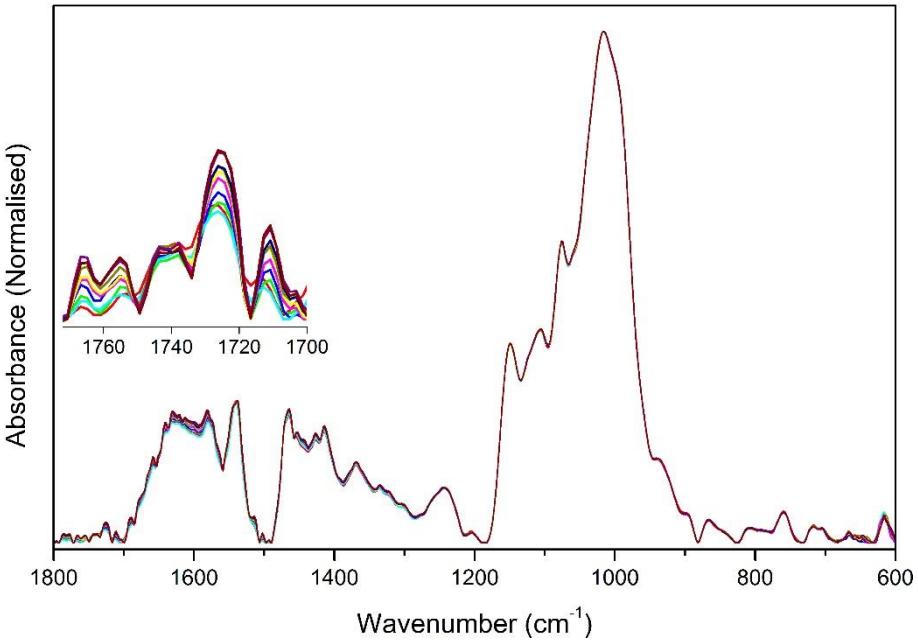

Figure S12: 10 replicate ATR-FTIR spectra of KGMG.

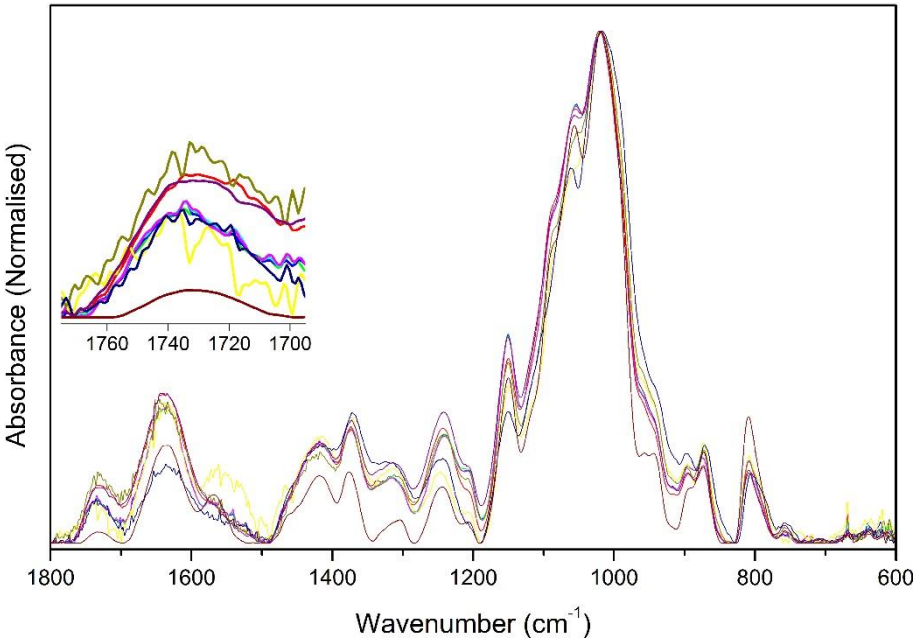

Figure S13: 10 replicate ATR-FTIR spectra of KGMB-ac.

Solid-state NMR spectroscopy

^{13}C NMR peak assignment

Table S6: Peak assignment for solid-state ^{13}C SPE-MAS NMR spectrum of KGM (see Figure 3b and Figure 4b for spectrum and labels). All chemical shift values are in ppm. Experimental chemical shifts δ_{exp} are compared to published ones δ_{lit} for KGM in solution in references 1 (Katsuraya et al., 2003) and 2 (Rakhimov, Shashkov, Zhauynbaeva, Malikova & Abdullaev, 2004), for KGM in the solid-state in reference 3 (Vieira & Gil, 2005), and for magnesium stearate in reference 4 (Delaney et al., 2017). *: associated with very low intensity signals in 24 to 39 ppm range.

Signal	δ_{exp}	Assignment	δ_{lit} (ref. 1)	δ_{lit} (ref. 2)	δ_{lit} (ref. 3)	δ_{lit} (ref. 4)
F	15	CH_3 of magnesium stearate				13-15
A	21	Acetyl CH_3	-	22		
G	33	CH_2 of magnesium stearate				31-34*
B	62	Mannose C6	62	62-64	62	
		Glucose C6	61	62-64		
C	74	Glucose C4	79	80	73	
		Mannose C4	77	74-78		
		Glucose C5	76	74-76		
		Mannose C5	76	74-77		
		Mannose C2	72	70-73		
		Glucose C2	74	74		
		Mannose C3	73	71-75		
		Glucose C3	76	75		
D	103	Glucose C1	104	104	102	
		Mannose C1	101	100-101		
E	173	Acetyl C=O		175		
H	182	C=O of magnesium stearate				179-188

^{13}C CP-MAS at different contact times T_{CP}

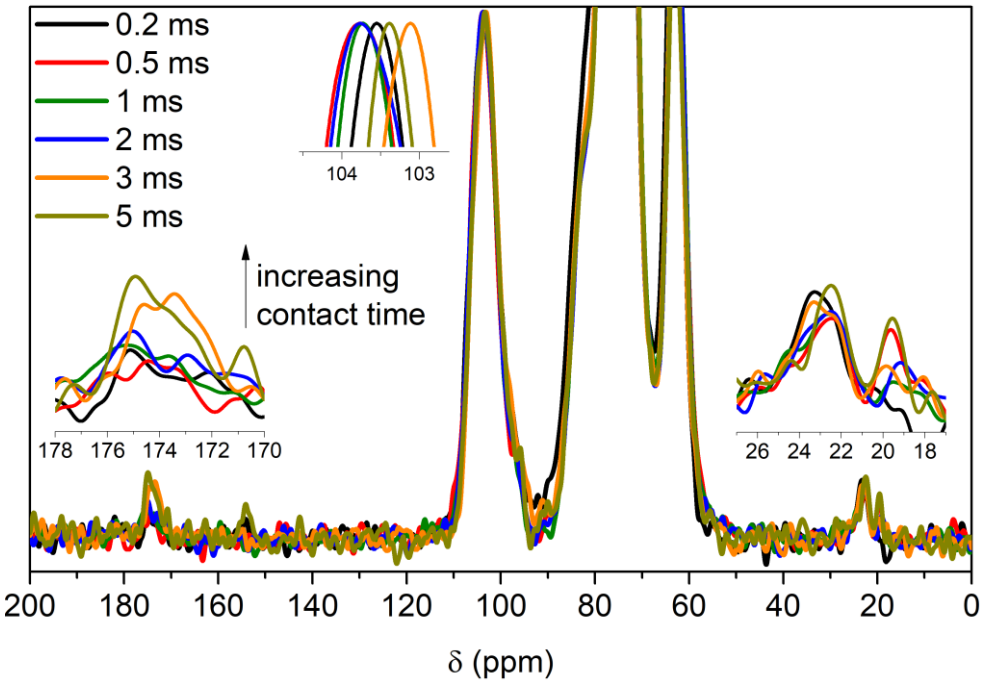

Figure S14: Solid-state ^{13}C CP-MAS NMR spectra of KGMA with different contact times T_{CP} (all spectra normalized to signal D at 103 ppm).

Resolution of signals A and D

Table S7: Resolution of chosen signals in ^{13}C CP-MAS and ^{13}C SPE-MAS NMR spectra determined with equation 3.

^{13}C NMR	CP-MAS		SPE-MAS
Signals	D and C (103 and 74 ppm)	A and G (21 and 33 ppm)	D and C (103 and 74 ppm)
KGMA	3.8	-	4.1
KGMB	3.8	-	4.0
KGMC	3.8	2.1	
KGMD	3.8	2.6	
KGME	3.8	-	4.1
KGMF	3.8	-	
KGMG	3.8	2.6	
KGMB-ac	4.1	-	5.7

Estimation of longitudinal relaxation times T_1

^{13}C longitudinal relaxation times (T_1) of KGMB-ac were estimated at 10 kHz MAS with one-dimensional inverse recovery experiments with a 7.4 µs 90° pulse length, for tested T_1 values of 5, 10 and 20 s, with 7,737, 3,846, and 5,836 scans, respectively.

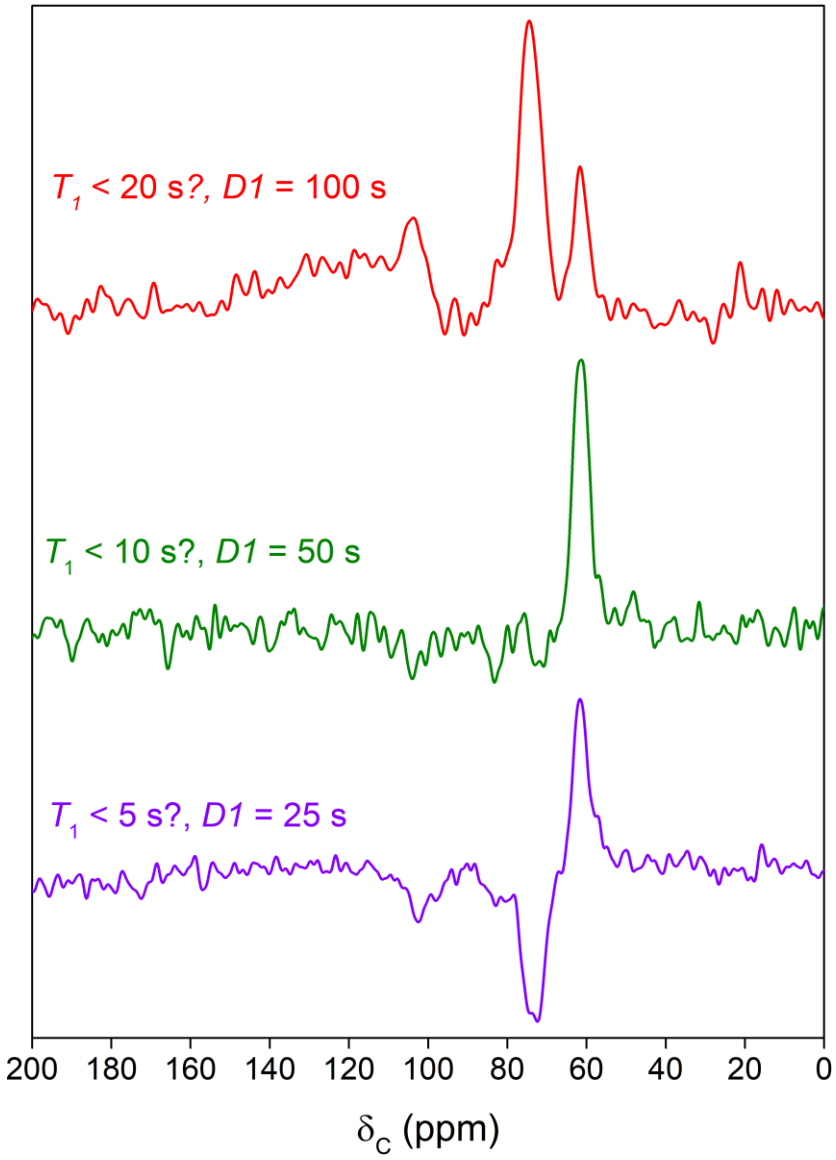

Figure S15: ^{13}C inversion recovery spectra for KGMB-ac, for different tested T_1 values (with different repetition delays D1, see Table S6 for ^{13}C NMR signal assignment).

Comparison of ^{13}C SPE-MAS and CP-MAS spectra of KGM samples

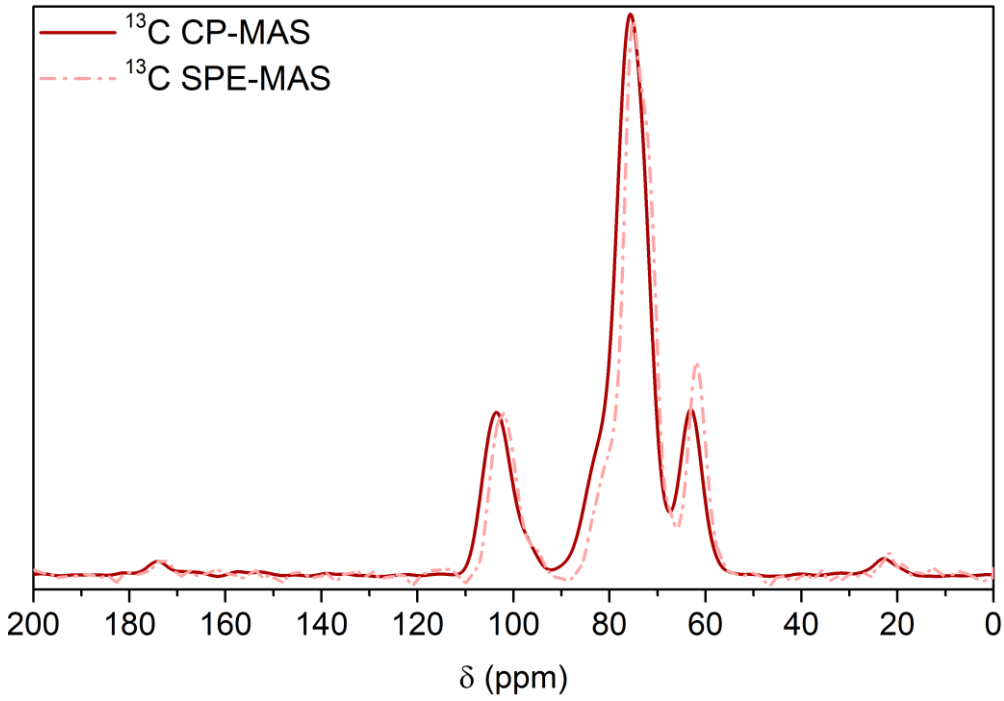

Figure S16: ^{13}C SPE-MAS (dashed-dotted line) and ^{13}C CP-MAS (solid line) spectra of KGMA (spectra normalized to signal D at 103 ppm).

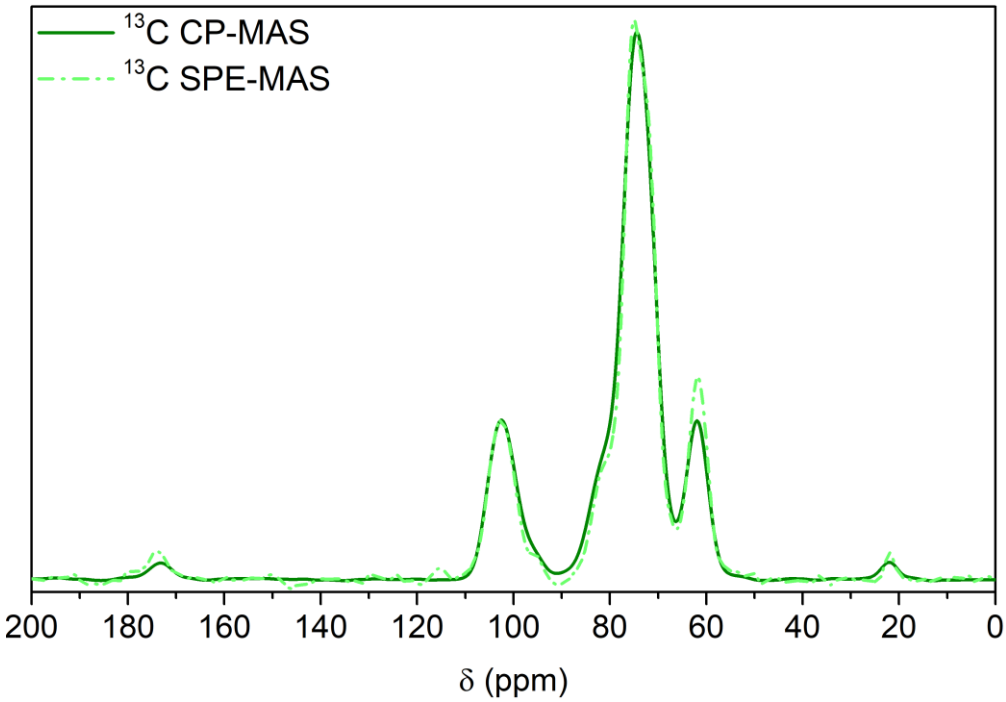

Figure S17: ^{13}C SPE-MAS (dashed-dotted line) and ^{13}C CP-MAS (solid line) spectra of KGMB (spectra normalized to signal D at 103 ppm).

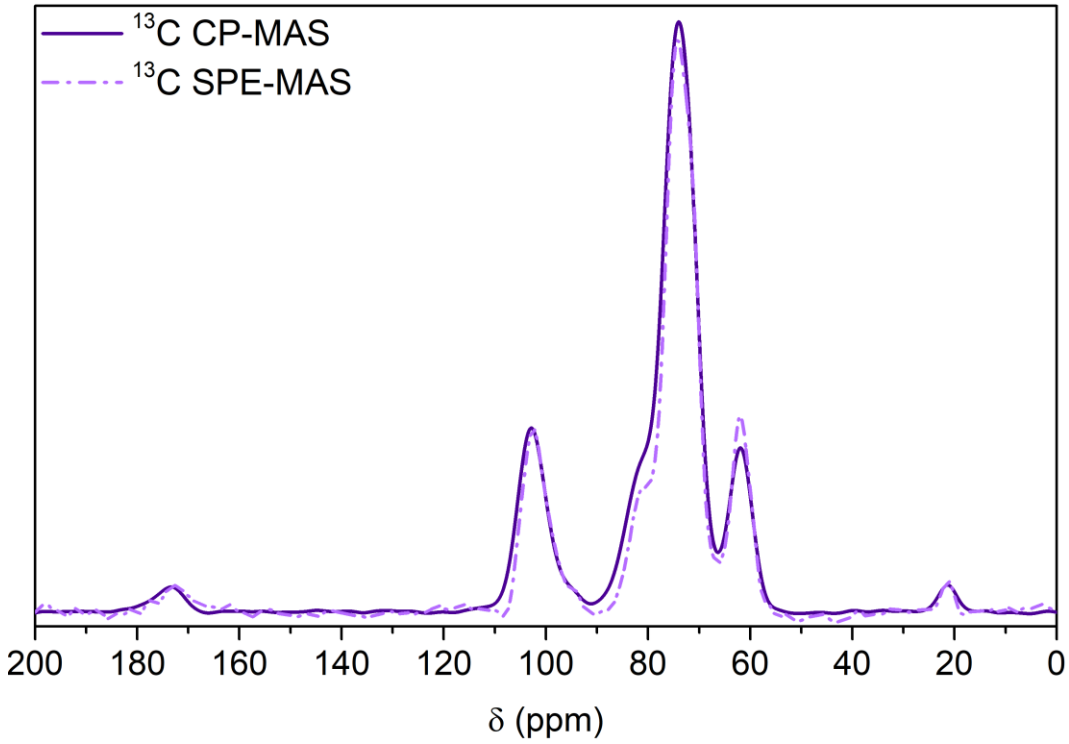

Figure S18: ^{13}C SPE-MAS (dashed-dotted line) and ^{13}C CP-MAS (solid line) spectra of KGMB-ac (spectra normalized to signal D at 103 ppm).

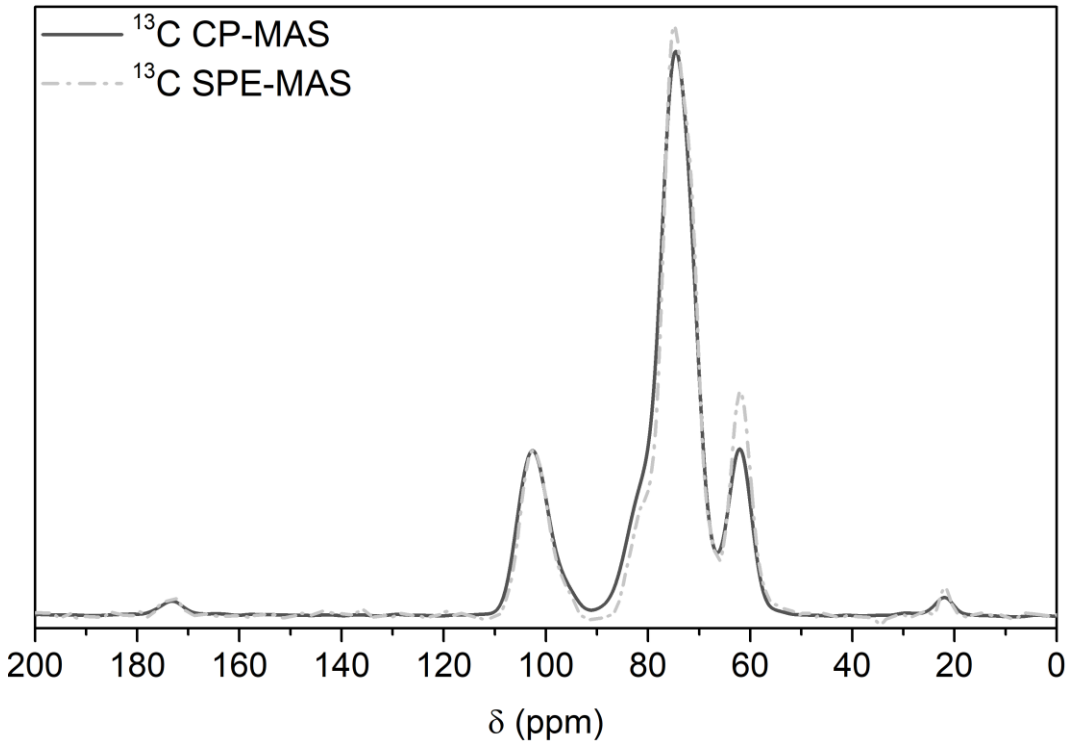

Figure S19: ^{13}C SPE-MAS (dashed-dotted line) and ^{13}C CP-MAS (solid line) spectra of KGME (spectra normalized to signal D at 103 ppm).

DA values from solid-state NMR and ATR-FTIR spectroscopy

Table S8: Overview of the *DA* values determined for KGM samples via ATR-FTIR, ^{13}C CP-MAS NMR and ^{13}C SPE-MAS NMR. Standard deviations were determined for DA_{IR} from 10 replicate measurements, for DA_{CP} and $DA_{SPE,q}$ through Equation 2 from the signal-to-noise ratio *SNR* of the acetyl group methyl signal.

Samples	DA_{IR} (a.u.)	DA_{CP} (a.u.)	*SNR* (CP)	$DA_{SPE,q}$ (%)	*SNR* (SPE)	$DA_{CP,q}$ (%)
KGMA	4.90 ± 0.57	7.82 ± 0.36	22	7.36 ± 2.53	4.8	7.32 ± 0.60
KGMB	5.70 ± 1.65	6.33 ± 0.26	24	4.81 ± 1.35	5.3	5.93 ± 0.47
KGMB-ac	10.01 ± 0.02	8.60 ± 0.48	19	8.11 ± 1.59	7.0	8.05 ± 0.70
KGMC	1.73 ± 0.32	4.76 ± 0.46	12	-	-	4.45 ± 0.53
KGMD	4.75 ± 1.16	5.64 ± 0.65	11	-	-	5.28 ± 0.70
KGME	10.69 ± 1.18	5.70 ± 4.72	21	6.44 ± 0.88	9.3	5.33 ± 0.44
KGMF	4.19 ± 0.53	4.42 ± 0.29	17	-	-	4.14 ± 0.39
KGMG	1.79 ± 0.34	7.68 ± 0.50	17	-	-	7.19 ± 0.67

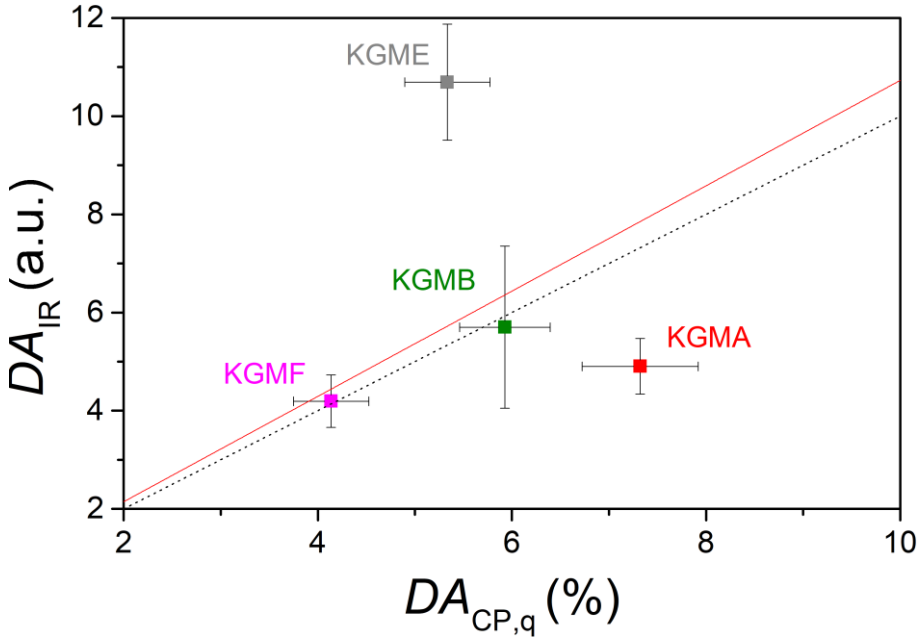

Figure S20: DA values of pure KGM samples determined from FTIR and CP methods (CP values corrected with calibration from SPE, Eq. 4 and 5), with their linear fit (y = (1.073 ± 0.290)x, R^2 = -0.30, solid red line), and the diagonal (dotted black line). The samples excluded from the fit are KGMC, KGMD and KGMG, which contain excipients including magnesium stearate, as well as KGMB-ac, which is not expected to be homogeneously acetylated following the acetylation reaction.

References

Chua, M., Chan, K., Hocking, T. J., Williams, P. A., Perry, C. J., & Baldwin, T. C. (2012). Methodologies for the extraction and analysis of konjac glucomannan from corms of Amorphophallus konjac K. Koch. *Carbohydr. Polym., 87*, 2202-2210.

Delaney, S. P., Nethercott, M. J., Mays, C. J., Winquist, N. T., Arthur, D., Calahan, J. L., Sethi, M., Pardue, D. S., Kim, J., Amidon, G., & Munson, E. J. (2017). Characterization of synthesized and commercial forms of magnesium stearate using differential scanning calorimetry, thermogravimetric analysis, powder X-ray diffraction, and solid-state NMR spectroscopy. *J. Pharm. Sci., 106*, 338-347.

Du, X., Li, J., Chen, J., & Li, B. (2012). Effect of degree of deacetylation on physicochemical and gelation properties of konjac glucomannan. *Food Res. Int., 46*, 270-278.

Hernandez, J. M., Gaborieau, M., Castignolles, P., Gidley, M. J., Myers, A. M., & Gilbert, R. G. (2008). Mechanistic investigation of a starch-branching enzyme using hydrodynamic volume SEC analysis. *Biomacromolecules, 9*, 954-965.

Katsuraya, K., Okuyama, K., Hatanaka, K., Oshima, R., Sato, T., & Matsuzaki, K. (2003). Constitution of konjac glucomannan: chemical analysis and 13C NMR spectroscopy. *Carbohydr. Polym., 53*, 183-189.

Kok, M. S., Abdelhameed, A. S., Ang, S., Morris, G. A., & Harding, S. E. (2009). A novel global hydrodynamic analysis of the molecular flexibility of the dietary fibre polysaccharide konjac glucomannan. *Food Hydrocoll., 23*, 1910-1917.

Liu, M. M., Fan, J. Y., Wang, K., & He, Z. (2007). Synthesis, characterization, and evaluation of phosphated cross-linked konjac glucomannan hydrogels for colon-targeted drug delivery. *Drug Deliv., 14*, 397-402.

McDonald, G. R., Hudson, A. L., Dunn, S. M. J., You, H., Baker, G. B., Whittal, R. M., Martin, J. W., Jha, A., Edmondson, D. E., & Holt, A. (2008). Bioactive contaminants leach from disposable laboratory plasticware. *Science, 322*, 917-917.

Mori, S. (1979). Contamination of water and organic solvents stored in plastic bottles with phthalate ester plasticizers. *108*, 325-332.

Nep, E. I., & Conway, B. R. (2012). Preformulation studies on grewia gum as a formulation excipient. *J. Therm. Anal. Calorim., 108*, 197-205.

Rakhimov, D. A., Shashkov, A. S., Zhauynbaeva, K. S., Malikova, M. K., & Abdullaev, N. D. (2004). Glucomannan from Narcissus poeticus studied by PMR and 13C NMR spectroscopy. *Chem. Nat. Comp., 40*, 358-361.

Sevenou, O., Hill, S. E., Farhat, I. A., & Mitchell, J. R. (2002). Organisation of the external region of the starch granule as determined by infrared spectroscopy. *Int. J. Biol. Macromol., 31*, 79-85.

Vieira, M., & Gil, A. (2005). A solid state NMR study of locust bean gum galactomannan and konjac glucomannan gels. *Carbohydr. Polym., 60,* 439-448.

Williams, M. A. K., Foster, T. J., Martin, D. R., Norton, I. T., Yoshimura, M., & Nishinari, K. (2000). A molecular description of the gelation mechanism of konjac mannan. *Biomacromolecules, 1,* 440-450.

Xu, Z. L., Yang, Y. H., Jiang, Y. M., Sun, Y. M., Shen, Y. D., & Pang, J. (2008). Synthesis and characterization of konjac glucomannan-graft-polyacrylamide via gamma-irradiation. *Molecules, 13,* 490-500.

Yu, H. Q., Huang, Y. H., Ying, H., & Xiao, C. B. (2007). Preparation and characterization of a quaternary ammonium derivative of konjac glucomannan. *Carbohydr. Polym., 69,* 29-40.